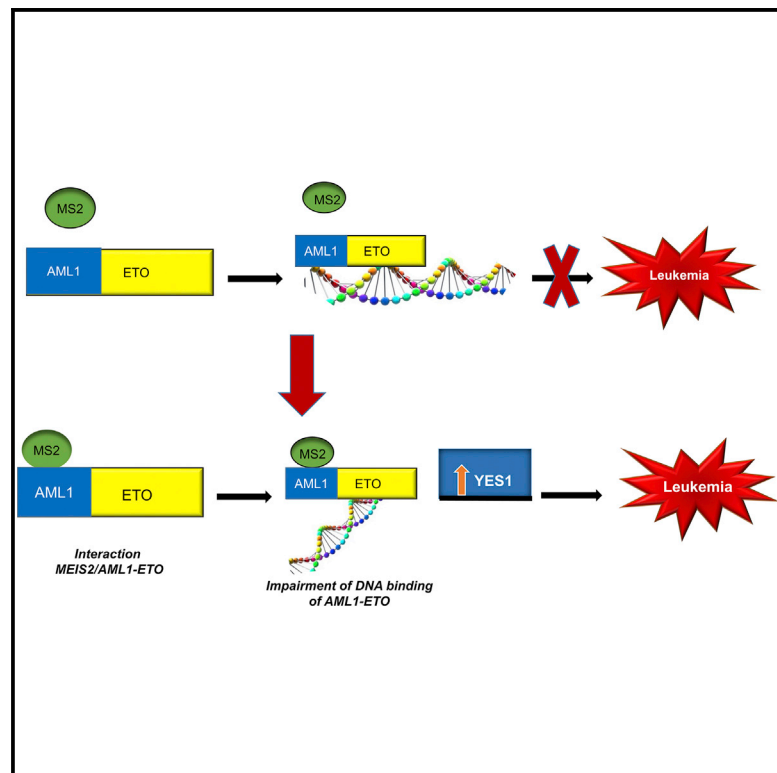


Cell Reports

MEIS2 Is an Oncogenic Partner in AML1-ETO-Positive AML

Graphical Abstract



Authors

Naidu M. Vegi, Josef Klappacher,
Franz Oswald, ...,
Hendrik G. Stunnenberg,
Michaela Feuring-Buske, Christian Buske

Correspondence

christian.buske@uni-ulm.de

In Brief

AML1-ETO is the most frequent fusion gene in human acute myeloid leukemia, but it is difficult to target therapeutically. Vegi et al. find that the homeobox gene MEIS2 is an oncogenic partner in AML1-ETO-positive AML. MEIS2 alters the DNA binding properties of AML1-ETO, resulting in reduced transcriptional repression of *YES1*, which is thus a possible therapeutic target.

Highlights

- *MEIS2* is aberrantly expressed in AML1-ETO AML
- Co-expression of MEIS2 with AML1-ETO induces AML in a murine model
- MEIS2 strongly binds to AML1-ETO
- MEIS2 increases YES1 expression by impairing AML1-ETO DNA binding

Accession Numbers

GSE81174

GSE81321

GSE81328

GSE81329



MEIS2 Is an Oncogenic Partner in AML1-ETO-Positive AML

Naidu M. Vegi,¹ Josef Klappacher,¹ Franz Oswald,² Medhanie A. Mulaw,¹ Amit Mandoli,³ Verena N. Thiel,² Shiva Bamezai,¹ Kristin Feder,¹ Joost H.A. Martens,³ Vijay P.S. Rawat,¹ Tamoghna Mandal,¹ Leticia Quintanilla-Martinez,⁴ Karsten Spiekermann,⁵ Wolfgang Hiddemann,⁵ Konstanze Döhner,⁶ Hartmut Döhner,⁶ Hendrik G. Stunnenberg,³ Michaela Feuring-Buske,⁶ and Christian Buske^{1,7,*}

¹Institute of Experimental Cancer Research, CCC and University Hospital of Ulm, 89081 Ulm, Germany

²Department of Internal Medicine I, Center for Internal Medicine, University Medical Center Ulm, Albert-Einstein-Allee 23, 89081 Ulm, Germany

³Department of Molecular Biology, Faculty of Science, Nijmegen Centre for Molecular Life Sciences, Radboud University, 6500HB Nijmegen, the Netherlands

⁴Institute of Pathology and Neuropathology, Eberhard Karls University of Tübingen and Comprehensive Cancer Center, University Hospital Tübingen, Liebermeisterstrasse 8, 72076 Tübingen, Germany

⁵Department of Internal Medicine III, University Hospital Grosshadern, Ludwig-Maximilians-University (LMU), 81377 Munich, Germany

⁶Department of Internal Medicine III, University Hospital Ulm, 89081 Ulm, Germany

⁷Core Facility Genomics, Medical Faculty Ulm, Ulm University, 89081 Ulm, Germany

*Correspondence: christian.buske@uni-ulm.de

<http://dx.doi.org/10.1016/j.celrep.2016.05.094>

SUMMARY

Homeobox genes are known to be key factors in leukemogenesis. Although the TALE family homeodomain factor *Meis1* has been linked to malignancy, a role for *MEIS2* is less clear. Here, we demonstrate that *MEIS2* is expressed at high levels in patients with AML1-ETO-positive acute myeloid leukemia and that growth of AML1-ETO-positive leukemia depends on *MEIS2* expression. In mice, *MEIS2* collaborates with AML1-ETO to induce acute myeloid leukemia. *MEIS2* binds strongly to the Runt domain of AML1-ETO, indicating a direct interaction between these transcription factors. High expression of *MEIS2* impairs repressive DNA binding of AML1-ETO, inducing increased expression of genes such as the druggable proto-oncogene *YES1*. Collectively, these data describe a pivotal role for *MEIS2* in AML1-ETO-induced leukemia.

INTRODUCTION

Aberrant expression of clustered homeobox genes, or *HOX* genes, is a molecular hallmark of acute myeloid leukemia (AML), and many experimental studies have proven that dysregulated expression of this highly conserved family of transcription factors is a key factor in leukemia development (Alharbi et al., 2013; Argiropoulos et al., 2007; Jung et al., 2015; McGonigle et al., 2008; Spencer et al., 2015). Besides *HOX* genes, non-clustered homeobox genes, such as the *ParaHox* gene *CDX2*, have been shown to play an essential role in leukemogenesis (Faber et al., 2013; Lengerke and Daley, 2012; Rawat et al., 2012), as have members of the three-amino-acid-loop extension

(TALE) superfamily, *MEIS1* and *PBX1* (Argiropoulos et al., 2007). The TALE superfamily is characterized by three highly conserved additional residues, proline-tyrosine-proline, in the first loop region of the homeodomain (Bürglin, 1997). So far, three functional *Meis* genes have been identified (*Meis1*, *Meis2*, and *Meis3*). *MEIS1* and *MEIS2* show 82% homology at the amino acid level. Homology is particularly high within the homeodomain and in a second conserved domain, the homothorax homology domain (Hth) (Moens and Selleri, 2006). There is a rich body of evidence arguing that *Meis1* plays a pivotal role in normal and malignant hematopoiesis. Murine transplantation models clearly showed that *Meis1* collaborates with native *Hox* genes such as *HoxA9* and *HoxA10* and multiple NUP98-HOX fusion genes in inducing AML (Kroon et al., 1998; Pineault et al., 2003; Thorsteinsdottir et al., 2001). Furthermore, *MEIS1* and multiple *HOX* genes are aberrantly expressed in a variety of human AML genotypes such as NPM1 mutated cytogenetically normal (CN)-AML or AML with complex karyotype (Kawagoe et al., 1999; Rawat et al., 2008). Interestingly, to date, *MEIS1* is the only *MEIS* family member to be implicated in normal or leukemic hematopoiesis. In this report, we characterize *MEIS2* as a potent oncogene in AML1-ETO (AE)-positive AML.

RESULTS

The Homeobox Gene *MEIS2* Is Aberrantly Expressed in Patients with AE-Positive AML

Because there are few reports on the expression and function of *MEIS2* in AML, expression of this gene was evaluated in a large cohort of patients with AML and normal CD34⁺ bone marrow (BM) cells by real-time qPCR (Table S1). Strikingly, *MEIS2* expression in AE-positive AML was significantly higher than in *PML-RARA* and *inv(16)* positive cases ($n = 11$) ($p < 0.0001$) (Figure 1A). There was also high expression in CN-AML, independent of the *NPM1* mutational status, an AML genotype

A

log₁₀ fold expression of MEIS2 (TBP)

○ = not expressed

22 fold ****

**

*

t(8:21) (n=50)

PML-RARA (n=6/11)

INV(16) (n=1/1)

NPM1^{WT}C (n=9)

NPM1^{WT}T (n=5)

nBMCDC34⁺ (n=7/13)

B

log₁₀ fold expression of MEIS2 (TBP)

○ = not expressed

t(8:21) (n=52)

CD34⁺CD38⁺ (n=3)

CD34⁺CD38⁺ (n=3)

CD34⁺CD38⁺ (n=2)

nBMCDC34⁺ (n=13)

CD34⁺CD38⁺ (n=5)

CD34⁺CD38⁺ (n=2)

CD34⁺CD38⁺ (n=5)

Leukemic

Normal

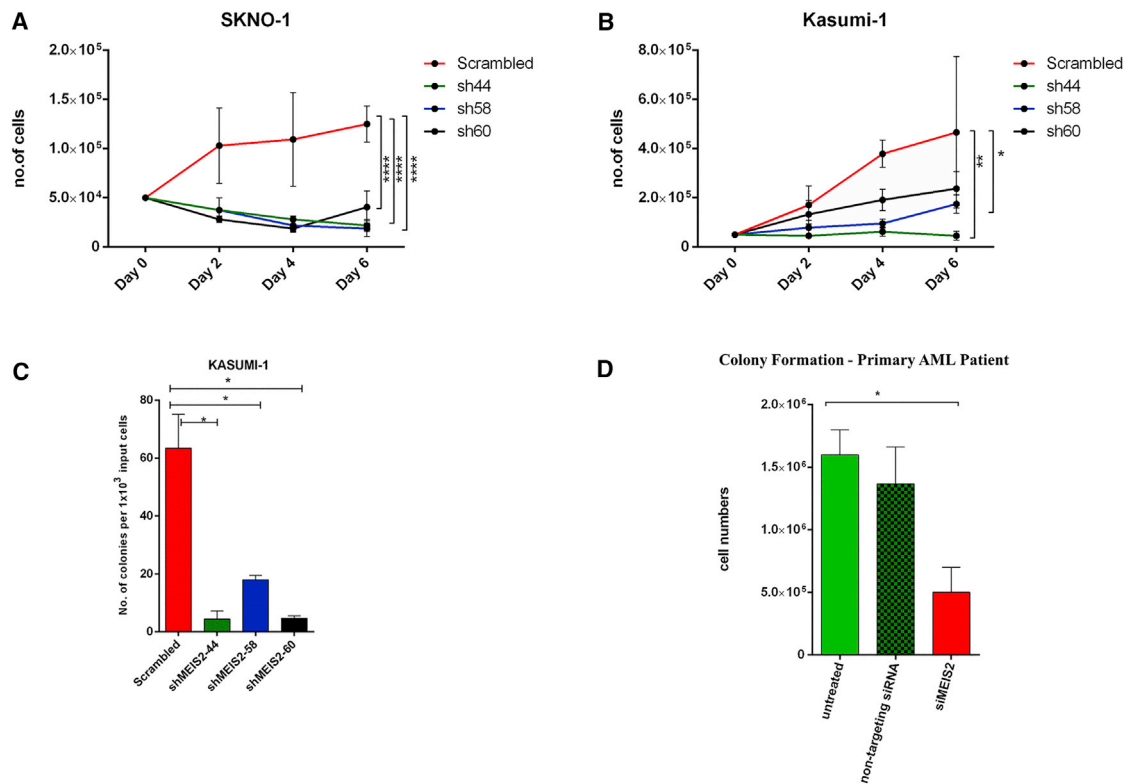


Figure 2. Impact of shRNA-Mediated Lentiviral Knockdown of *MEIS2* on t(8;21)-Positive AML Cell Lines and a t(8;21)-Positive Patient Sample

(A and B) Impact of knockdown (KD) of *MEIS2* compared to SCR control on (A) proliferation ($n = 3$ for SKNO-1 with KD of 31.85 ± 8.4 SEM for sh44, 43.8 ± 6.8 SEM for sh58, and 19.5 ± 2.78 SEM for sh60, respectively, and 42.7 ± 7.1 SEM for sh44, 30.5 ± 4.4 SEM, for sh58 and 30.9 ± 6.3 SEM for sh60, respectively) and (C) colony formation ($n = 3$ for Kasumi-1). Significance was calculated by two-way ANOVA (**** $p < 0.0001$; *** $p = 0.001$; * $p = 0.005$).

(D) Impact of siRNA-mediated knockdown of *MEIS2* in a diagnostic, previously untreated patient sample having, as a sole cytogenetic abnormality, the translocation t(8;21) (no. 62 in Table S1) on cell number compared to SCR control ($n = 1$ in technical triplicates). Average knockdown efficiency was 54.2%; cell viability was measured 72 hr after siRNA induction.

in the retroviral tagged cancer genes database (RTCGD) (data not shown).

To characterize genes and pathways differentially expressed by overexpression of *MEIS2* and *AE*-positive cells, we performed microarray analyses 48 hr after successful gene transduction in 5-fluorouracil (5-FU)-mobilized murine progenitor cells. In comparison to the GFP control, *MEIS2* with *AE* induced upregulation of 75 probesets corresponding to 23 genes and downregulation of 159 probesets corresponding to 122 genes. In contrast to the upregulated genes, the vast majority of down-regulated genes did not overlap between *AE/MEIS2* and *AE* alone (Figures S3A and S3B; Table S4). When these differentially expressed genes between *AE/MEIS2* and GFP were analyzed in the Kyoto Encyclopedia of Genes and Genomes (KEGG)-based pathway analysis, “cytokine-cytokine receptor interaction,” “transcriptional misregulation in cancer,” and “pathways in cancer” scored among the top-five ranking categories. In a direct comparison between *AE* and *AE/MEIS2* BM, out of 195 differentially regulated probesets referring to 145 genes, 29 probesets (12 genes) were upregulated and 166 probesets (80 genes) were downregulated (Table S4). Interestingly, *Hoxa* genes such as *Hoxa5*, *Hoxa7*, *Hoxa9*, and *Hoxa10* were downregulated

in *AE* and *AE/MEIS2* compared to the empty vector. This was further validated by qRT-PCR, indicating that the leukemogenicity of *AE/MEIS2* does not depend on upregulation of oncogenic *Hoxa* genes (Figures S3C and S3D). Gene set enrichment analysis (GSEA) analysis for oncogenic signature (MsigDB version 5.0) showed enrichment for gene sets such as “*JAK2*” and “*PTEN*” in *AE/MEIS2* versus *AE* alone (Figure S3E; Table S4). Consistent with the finding that *MEIS2* did not increase leukemogenicity of *AE9a*, RNA-seq of leukemic BM showed a close overlap in gene expression between *AE9a* and *AE9a/MEIS2*, indicating that adding of *MEIS2* to the leukemogenic truncated *AE9a* does not induce gross changes in the molecular phenotype of *AE9a*-positive leukemias (Figures S3F and S3G).

Taken together, these data indicate that *MEIS2* functionally collaborates with *AE* in AML.

MEIS2 Binds to AE

To understand the mechanism of *AE-MEIS2* collaboration, we first sought to identify domains of the fusion gene that may be critical for collaboration between *AE* and *MEIS2* using the CFU-S assay as readout for growth-promoting activity (Figures S4A and S4B). Only the inactivating point mutation in the Runt

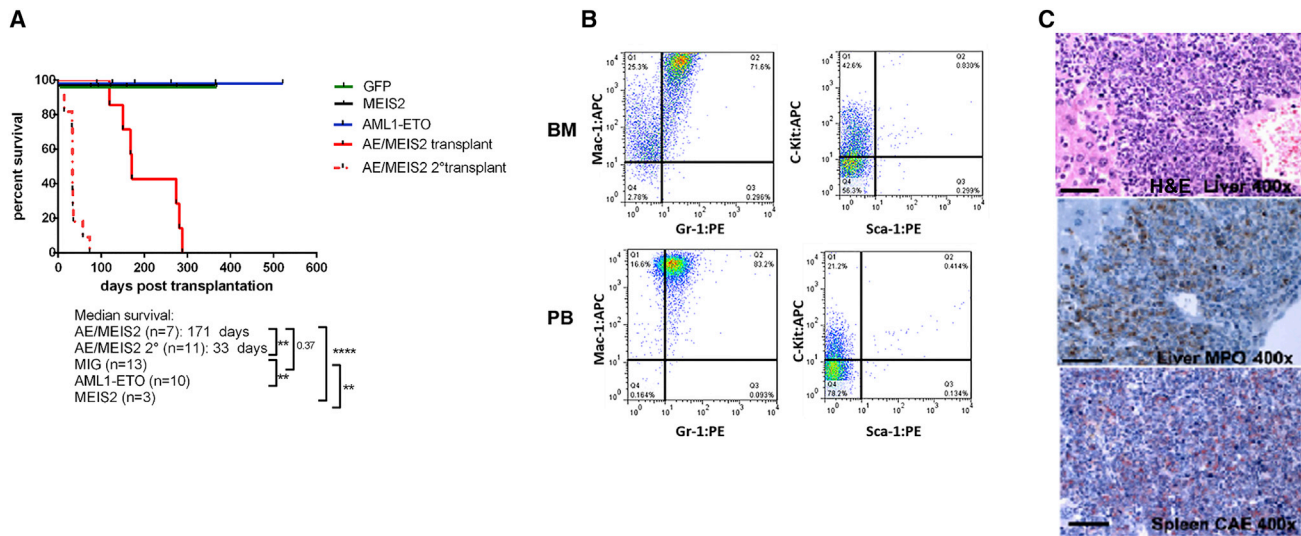


Figure 3. Co-expression of MEIS2 and AML1-ETO Induces AML in Mice

(A) Survival plot of mice transplanted with AE and MEIS2. Kaplan-Meier survival curves of mice transplanted with BM cells expressing AML1-ETO (AE), MEIS2, the empty GFP control vector, or AE/MEIS2. Survival of secondary recipients transplanted with BM of diseased primary AE/MEIS2 mice is shown in addition. Log-rank Mantle-Cox test was used to calculate the statistical significance as indicated (**p < 0.005; ****p < 0.0001; ***p = 0.0001; **p = 0.001).

(B and C) Dot plot of a representative leukemic AE/MEIS2 mouse (B) and histological analysis of different organs (C). Immunophenotyping and histology of BM and PB of a representative mouse diagnosed with AML is given (mouse no. 10; Table S3). Samples were gated for GFP-positive cells. MPO, myeloperoxidase; CAE, N-acetyl-chloroacetate esterase. Histology pictures are magnified 400 \times . Scale bar, 50 μ m.

domain, not deletion of the NHR1 or C-terminal stretch, reduced collaboration between MEIS2 and the fusion gene, indicating that DNA binding properties are crucial for AE-MEIS2 leukemogenic collaboration. There was a trend that MEIS2 could further enhance CFU-S activity of the C-terminally truncated Δ 540 AE construct that contains the TAF/NHR1 domain and lacks the zinc-finger domains, previously shown to have similar activity as the wild-type AE (Westendorf et al., 1998) (Figure S4C). To test for a possible direct interaction between AE and MEIS2, co-immunoprecipitation (coIP) assays along with various other mutants of MEIS2 (Figure S4D) were performed in HEK293 cells. Surprisingly, strong binding of MEIS2 to the Runt domain of AE could be documented (Figures 4A and 4B). Additional experiments showed that AE9a is also able to strongly bind to MEIS2 (Figure S4E) and that the N-terminal region (amino acids [aa] Δ 1–68 or 69–470) of MEIS2 is critical for binding to the Runt domain of AE and AE9a (Figures 4C, 4D, S4E, and S4F). The binding of MEIS2 to AE was validated in a human leukemic background by performing immunoprecipitation for ETO and western blotting for MEIS2 in the AE-positive human cell line SKNO-1 (Figure S4G). To test whether hematopoietic activity of MEIS2 depends on binding to AE, we generated a mutant with deletion of 1–68 aa N-terminally (MEIS2(69–470)), which has lost its binding capacity to the fusion gene (Figure 4D). In contrast to the wild-type MEIS2, which induced significantly more colonies in collaboration with AE than AE alone, MEIS2(69–470) plus AE failed to increase colony numbers compared to AE alone. This could be re-confirmed in secondary re-plating assays, which also showed a significant loss of activity of the AE/MEIS2 (69–470) combination compared to AE/MEIS2. Similarly, at the level of CFU-S, AE/MEIS2 increased spleen colony numbers signifi-

cantly compared to AE alone in contrast to the AE/MEIS2 (69–470) combination. This was further confirmed in the more sensitive Δ CFU-S assay, which showed a lack of collaboration between AE and MEIS2 (69–470) (Figures S4H–S4J). Collectively, these data provide evidence that MEIS2 is able to directly interact with the most frequent fusion gene in AML and that binding to AE is critical for its full collaborative activity in the CFU-S assay.

MEIS2 Alters Target Gene Binding of AE

To analyze whether MEIS2 expression levels impact AE DNA binding properties, chromatin immunoprecipitation (ChIP) sequencing was performed in the human AE-positive Kasumi cell line after shRNA-mediated MEIS2 knockdown (shMEIS2-44) compared to the scrambled control, using an AE fusion-specific antibody (Martens et al., 2012). Successful enrichment for AE target genes by the antibody used was first validated by ChIP qPCR for known specific binding partners of AE such as *SPI1*, *OGG1*, *FUT7*, and *NFE2*, each of which showed substantial enrichment (showing an up to 18-fold) (Figures S5A and S5B). In addition, motif analyses of the AE binding sites in the ChIP-seq revealed enrichment for both the *RUNX1* and *ETS1* target sites as previously reported (Martens et al., 2012) in both experimental arms, comprising between 35% and 42% of all target regions, as well as the presence of weaker motifs with 44.32% and 65.8% for scrambled (SCR) and shMEIS2, respectively (Figures S5C–S5F; Table S5). As we observed increased binding of AE to *RUNX1* after MEIS2 knockdown, changes in expression of *RUNX1* were tested in the t(8;21)-positive cell lines SKNO-1 and Kasumi after MEIS2 depletion: however, knockdown induced no major change of *RUNX1* expression in both cell lines (n = 3) (data not shown).

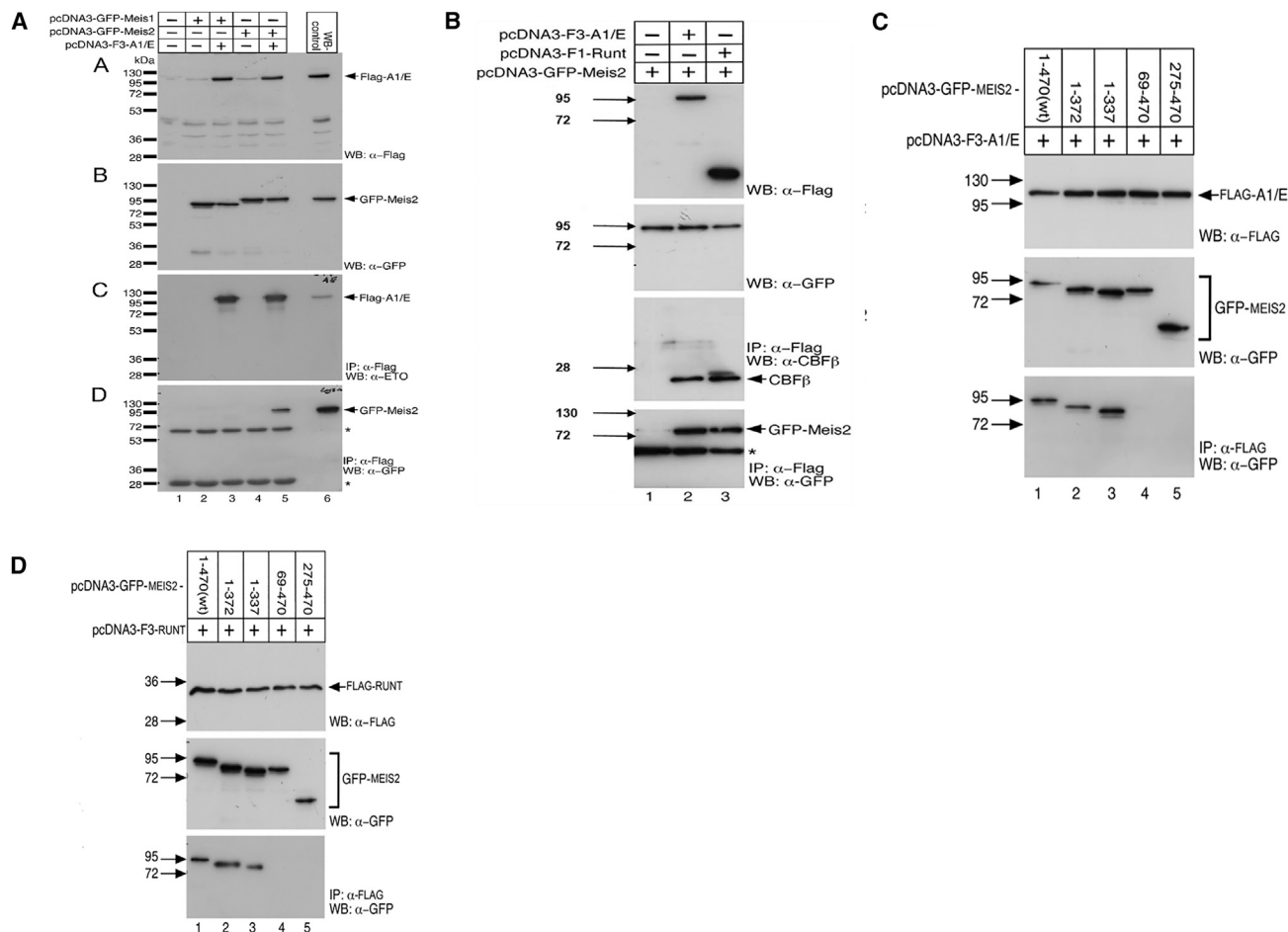


Figure 4. Co-immunoprecipitation Assays on AE and MEIS2 Interaction in HEK293 Cells

(A) Immunoprecipitation (IP) of FLAG-AE and western blot using anti-FLAG and anti-ETO (for AE) and anti-GFP (for MEIS2) antibodies, respectively. Interaction of MEIS2 with AE is shown in lane 5.

(B) IP of FLAG-RUNT and FLAG-AE and western blot using anti-FLAG (for RUNT and AE) and anti-GFP (for MEIS2) antibodies, respectively. MEIS2 interacts with AE and to the RUNT domain of AE (lane 3). *Immunoglobulin G (IgG) heavy chains (in C heavy and light IgG chains).

(C and D) Additional mutants of MEIS2 were generated to map the interacting domain of full-length AE and RUNT with MEIS2. WT MEIS2 and all the mutants interacted strongly with AE and RUNT, except the N-terminally deleted mutants $\Delta 1-68$ (aa 49-470) and $\Delta 1-274$ (aa 275-470).

At a cutoff of ≥ 10 -fold with a FDR rate threshold of 0.001 and a FDR effective Poisson threshold of 0, a total of 13,003 high-confidence DNA binding regions for AE with or without expression of shMEIS2 were detectable. Of note, knockdown of MEIS2 increased the number of AE binding sites compared to the control by >2 -fold. In addition, knockdown of the MEIS2 gene induced $>7,900$ unique AE binding sites, indicating gross changes in the DNA binding behavior of the fusion gene after MEIS2 depletion (Figure 5A). When we focused on the promoter regions (defined as binding regions 1 kb upstream and 100 bp downstream of the transcription start site), AE still bound to significantly more DNA sites after MEIS2 knockdown, with $>1,100$ unique binding sites compared to the control (Figure 5B; Table S4). The higher number of AE DNA binding sites after MEIS2 depletion was a consistent characteristic throughout the differentially annotated DNA regions (Figure 5C). Among those genes that showed substantial increase of AE binding af-

ter MEIS2 knockdown were *IGFBP7*, *mir-4442*, *OGG1*, *RUNX1*, and *WT1*. A smaller proportion of genes showed decreased AE binding after MEIS2 depletion, such as *mir-145*, *NDUFA4*, and *KRAS* (Figure S6A). Other genes did not meet the above-mentioned criteria for AE binding in the scrambled control but met the requirements with a >10 -fold increase in AE binding, such as *ASLX2*, *FLT3*, *CREB1*, *GSK3a*, and *HMGA1* (Table S6). Of note, expression of MEIS2 decreased after AE shRNA-mediated knockdown in SKNO-1 cells, although there was no documented binding of AE to the MEIS2 promoter (Figures S6B and S6C).

Thus, these data demonstrated that high MEIS2 expression is associated with a reduction of AE binding to DNA targets and, vice versa, that knockdown of MEIS2 increases AE binding sites. Furthermore, the data show that AE binds to a distinct and unique set of DNA sites in human AML cells when MEIS2 is highly expressed.

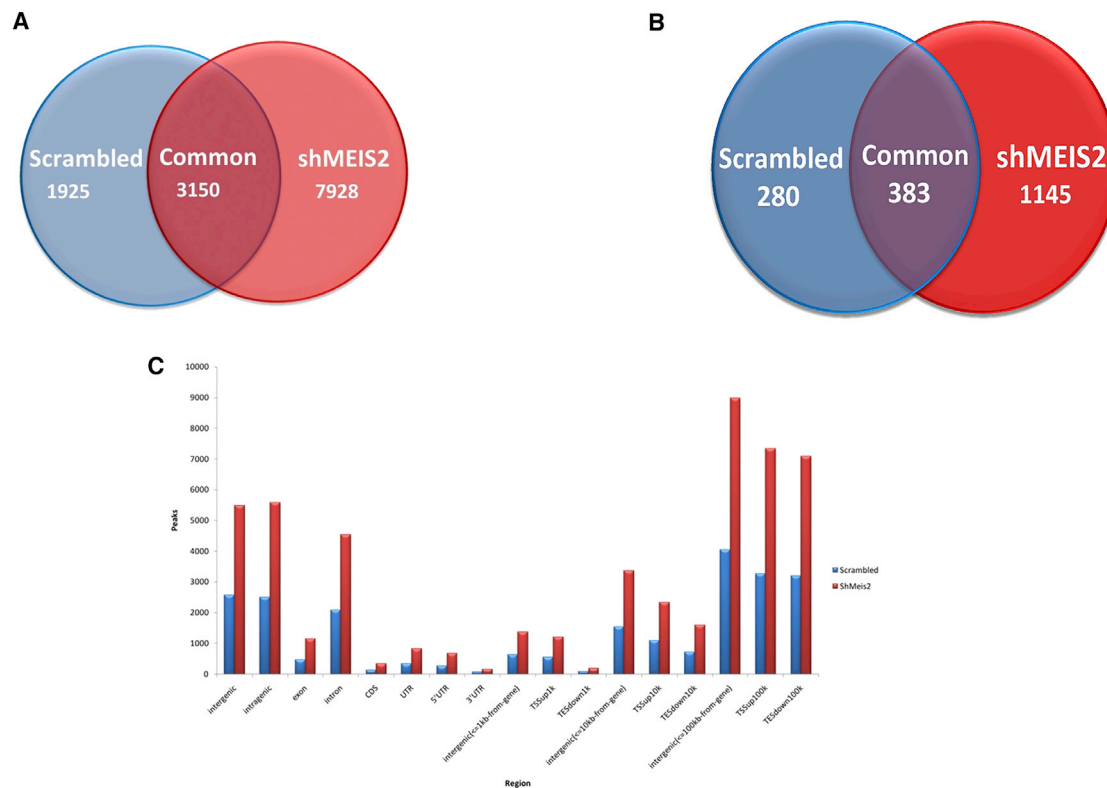


Figure 5. AE Binding Sites

(A) Venn diagram showing the number and overlap of all genomic AE binding sites in Kasumi-1 cells after knockdown of MEIS2 (shMEIS2-44) compared to the SCR control.

(B) Venn diagram showing the number and overlap of genomic AE binding sites in the promoter region (the annotated peaks that are 1 kb upstream of the TSS and 100 bp downstream of the TSS) in Kasumi-1 cells after knockdown of MEIS2 (shMEIS2-44) compared to the SCR control.

(C) Distribution of the AE binding sites in the genome (relative to RefSeq genes). TSS, transcriptional start site; TES, transcriptional end site.

High Expression of MEIS2 Is Associated with Loss of AE Binding to the YES1 Promoter Region and Increased YES1 Expression

To correlate AE target gene binding with expression levels, RNA-seq was performed in parallel to ChIP sequencing (ChIP-seq) for the same samples in duplicates. Genes were considered as differentially expressed when the difference in FPKM (fragments per kilobase per millions reads) was significant at a p value of 0.05, with a false discovery rate (FDR) of 0.05. First, differentially expressed genes were analyzed independent of AE target binding: 868 genes were differentially expressed between Kasumi cells transduced with the *MEIS2* shRNA versus scrambled control (Table S4). KEGG analysis showed changes in the expression of genes belonging to the categories ribosomes, lysosomes, and adherence junction (Tables S4 and S7). Of note, *MEIS2* knockdown induced major differences in gene expression, with an up to 2.25 log₂ fold change for upregulated genes (n = 365) and up to 9 log₂ fold for downregulated genes (n = 123 genes) compared to the SCR control (Table S4).

As a second step, we correlated differentially expressed genes with AE DNA binding. Among the genes with changes in expression and AE binding, there were two categories. The first showed an increase in expression accompanied by an enhanced

AE binding to their promoter region (e.g., *MPO*, *KIT*, *NUCB2*, and *CD34 MYOG1*). The second group showed decreased expression level parallel to increased AE binding (e.g., *YES1*, *BCL2L1*, *HMGAI*, *IGFBP2*, and *TXNIP*) after *MEIS2* knockdown (Table S8). We validated these findings for selected genes and found a significant (p < 0.05) positive correlation between expression levels determined by RNA-seq and qRT-PCR (Figure S6D). There was no decrease in the expression of the targetable receptor tyrosine kinases c-Kit and *FLT3* after *MEIS2* knockdown as validated by qRT-PCR. In contrast, knockdown of *MEIS2* induced a substantial decrease in expression of the Src kinase *YES1* accompanied by increased AE promoter binding of this gene (Figure 6A). This finding thus provided an intriguing gene whose expression was strongly dependent on MEIS2 overexpression and whose effects were potentially druggable. Of note, knockdown of *YES1* resulted in an up to 78% reduction in proliferation and 95% reduction in clonogenic growth in Kasumi cells (Figures 6B–6D), indicating that *YES1* expression is relevant for the cell growth of this AE-positive AML cell line. This was in line with the observation that knockdown of *Yes1* in primary leukemic murine AE9a/MEIS2 cells impaired primary clonogenic growth by, on average, 70.5% (sh84) and 71.14% (sh152) and re-plating by 93.98% and 69.13% for the two

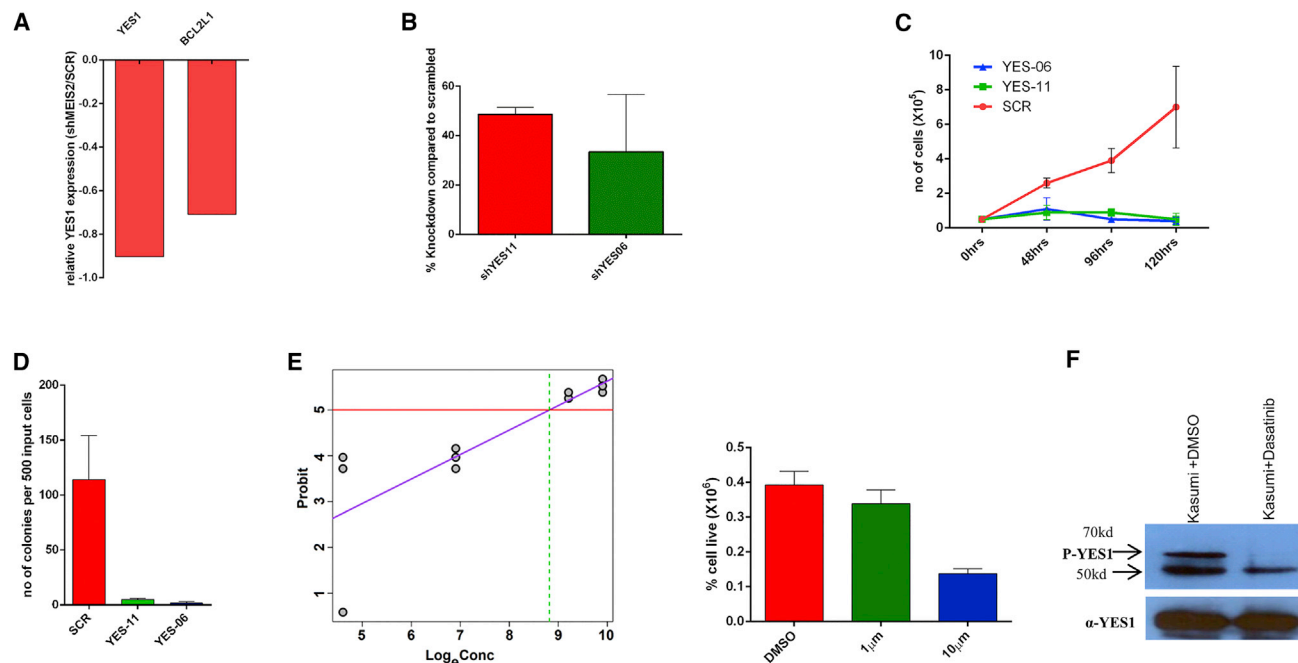


Figure 6. YES1 Expression after MEIS2 Knockdown

(A) Expression of YES1 after MEIS2 knockdown in Kasumi cells determined by qRT-PCR and RNA-seq showing downregulation of the kinase.

(B) Percentage of YES1 knockdown in Kasumi cells.

(C) Cell growth of Kasumi cells after YES1 knockdown compared to SCR control ($n = 3$).

(D) Colony formation after YES1 knockdown compared to SCR control ($n = 3$; mean \pm SEM).

(E) 2×10^5 Kasumi-1 cells were treated with dasatinib at different concentrations for 72 hr, resulting in an IC_{50} value of 6.8 μ M (calculated on the basis of live cells with probit = 5 [50% effect]; $Y = 0.53 \log_{10}$ concentration + 0.28 sigmoid model). Bar graphs (mean \pm SEM) show that dasatinib concentrations between 1,000 nm and 10,000 nm resulted in >50% cell growth inhibition after 72 hr.

(F) IP of YES1 and western blotting for p-YES1 in Kasumi-1 cells treated with DMSO or 6.8 μ M dasatinib for 72 hr, demonstrating loss of phosphorylation after dasatinib treatment.

shRNAs, respectively (Figures S6F–S6H). Indeed, all AML genotypes, including the AE-positive AML subtype showed YES1 expression as previously indicated in The Cancer Genome Atlas (TCGA) database (Network, 2013) (Figure S6E). Next, we tested the efficacy of pharmacological YES1 inhibition. So far, there are no selective YES1 inhibitors available. One of the most potent YES1 inhibitors is dasatinib, which also impairs other kinases such as c-Src, Fyn, and Lyn (BMS-354825) (Patel et al., 2013). The AE-positive Kasumi cell line, expressing high levels of MEIS2, is also positive for YES1 expression and showed complete loss of phosphorylation of the kinase after dasatinib treatment. With a half maximal inhibitory concentration (IC_{50}) value of 6.8 μ M, dasatinib was highly efficient in impairing Kasumi cell growth in vitro (Figures 6E and 6F). Although it has to be taken into account that dasatinib is a multitargeted kinase inhibitor known to target several other kinases such as Lyn, PDGFR, KIT, Lck, Fyn, and c-Src, these data at least suggest that YES1 is an attractive target in AE-positive AML.

All together, these data point to a regulatory network, in which high MEIS2 expression collaborates with AE in inducing leukemia, involving at least in part MEIS2's ability to strongly bind to AE and thereby grossly change binding of AE to its target genes on a global scale. This results in loss of repression of proto-oncogenes, exemplified by an increase in the expression of the YES1 kinase in

AML cells, thereby opening avenues to link a leukemogenic liaison between transcription factors to a druggable target.

DISCUSSION

AML characterized by the translocation t(8;21) counts for 15% of all human AML cases and is characterized by expression of the most frequent fusion gene detectable in patients with this disease. So far, the AE-positive AML genotype was not associated with deregulated homeobox gene expression (Andreeff et al., 2008; Lo et al., 2012). In this report, we now provide evidence that TALE homeobox genes are involved in AE leukemogenesis and that they can directly interact with the fusion gene. We initiated the study quantifying the expression of the TALE homeobox gene MEIS2 in a larger AML patient cohort and could readily demonstrate that MEIS2 is aberrantly highly expressed not only in virtually all AE-positive AML cases compared to normal CD34⁺ hematopoiesis but also in comparison to other core binding factor (CBF) leukemias. The mechanism behind this observation is unclear. Despite the gross differences in MEIS2 expression between AE AML samples and normal CD34⁺ BM cells, both populations did not show any major methylation differences at the CpG regions of the MEIS2 promoter as determined by MassARRAY technology, indicating that expression of this gene is not regulated by

methylation, at least of these CpG islands (data not shown). Interestingly, published microarray data documented a significantly and 4.3-fold (\log_2) increased expression of *MEIS2* after retrovirally induced overexpression of AE in human CD34⁺ cord blood cells compared to the control (expression atlas EMBL-EBI; Krejci et al., 2008), in line with our own data showing the same observation for murine progenitor cells, whereas in the human setting, a reduction of *MEIS2* expression after knockdown of AE was only observed in the t(8;21)-positive SKNO-1 cell line and not in Kasumi cells (data not shown). The mechanism of this is not clear, as we did not see any major binding of AE to the *MEIS2* region, as also described by Ptasinska et al. (Ptasinska et al., 2012).

Functional relevance of high *MEIS2* expression in collaboration with AE could be clearly demonstrated by knockdown in human AML cells and in the BM transplantation assay, in which only *MEIS2*, in collaboration with AE, induced leukemia in contrast to *MEIS2* or AE alone, as shown by us and several other groups (de Guzman et al., 2002; Fenske et al., 2004; Licht, 2001; Schessl et al., 2005). However, in our model, the latency time until development to AML was long, with a median time of 171 days until disease post-transplant. The long latency suggests that *MEIS2* in concert with the human full-length AE fusion gene needs additional partners. To test how this homeobox gene might functionally interconnect with AE, we analyzed binding between the two proteins and surprisingly found strong binding between *MEIS2* and AE. Interaction between endogenous *MEIS2* and AE could be re-confirmed in the human AML SKNO-1 cell line. These results thus implicate a previously unrecognized direct interaction between AE and *MEIS2* in human AML. An important question is whether direct binding to AE is relevant for the collaboration between *MEIS2* and AE. To address this, we generated a mutant that lost binding to AE. Importantly, this construct showed reduced hematopoietic activity compared to the full-length protein. *MEIS2* was also highly expressed in AML cases with NPM1 mutation or normal karyotype with an NPM1 wild-type protein, and shRNA-mediated knockdown of *MEIS2* impaired growth in a panel of AML cell lines harboring, among others, NPM1 mutation or a MLL fusion (data not shown). This might indicate that high *MEIS2* expression contributes to leukemogenesis in other AML genotypes. It will be important in future work to analyze this in more detail and to understand possible AE-independent mechanisms of *MEIS2* leukemogenicity. We also tested binding of *MEIS2* to the truncated AE9a oncogene and proved that *MEIS2* is also able to bind strongly to this AE isoform. However, we did not see acceleration of AE9a induced disease by *MEIS2* co-expression, in line with published data demonstrating rapid onset of leukemia by AE9a alone in contrast to the full-length AE fusion (Yan et al., 2006). Complex formation between TALE homeobox genes such as *Meis1* and *Pbx1* has been described and is essential for mediating *Hoxa9* leukemogenicity (Kroon et al., 1998; Shen et al., 1999), but so far, there are no reports on complex formation between TALE homeobox genes and the AE fusion gene. With regard to AE, the fusion gene might have a completely different DNA occupancy when interacting with *MEIS* proteins. Indeed, we could demonstrate that AE changes its DNA binding properties significantly after shRNA-mediated *MEIS2* knockdown in human AML cells. According to the ChIP-seq data presented in this work, AE DNA binding occupancy in

AML cells was substantially reduced when *MEIS2* was highly expressed. Conversely, *MEIS2* knockdown resulted in a gross and >100% increase in the number of AE binding sites, accompanied by a significant impairment of AML cell growth. This suggests that *MEIS2* might promote AE-associated leukemogenesis by impairing or restricting binding of a repressive AE complex to proto-oncogenes, resulting in a critical increase of potentially oncogenic AE targets (Ptasinska et al., 2012). This increase in AE binding was observed for several known genes involved in cell activation, growth, and cancer such as *KIT*, *MPO*, *HMGA1*, *CD34*, and *IGFBP7* (Ptasinska et al., 2012) or *YES1* and *MAPK1* (Maiques-Diaz et al., 2012). However, changes in AE binding to *KIT* did not result in changed expression in contrast to *YES1*. This SCRSrc kinase has previously been described as one of the key members of a gene set of AE targets with an AML1 binding site, co-occupied by the histone deacetylase 1 and characterized by a dramatic loss of H4 hyperacetylation marks. Interestingly, this study classified *YES1* among the target genes of AE (Maiques-Diaz et al., 2012). We could also demonstrate that high expression of *MEIS2* can impair AE binding to the *YES1* promoter, resulting in an increased expression of this proto-oncogene in human AML cells. Additionally, knockdown of *YES1* abrogated the growth of AE-positive AML as well as primary leukemic BM. Unfortunately, to date, no selective *YES1* kinase inhibitor is available. Among the most potent *YES1* inhibitors is dasatinib, which also blocks other src kinases (Patel et al., 2013). Although the data have to be interpreted with caution based on this, dasatinib a highly potent blocker of growth of AE-positive cells, and this was accompanied by dephosphorylation of the *YES1* protein. Interestingly, clinical trials are ongoing in AE-positive AML to test the efficacy of dasatinib as an addition to chemotherapy or as a single agent (Boissel et al., 2015; Marcucci et al., 2013). All of this illustrates that the leukemogenic collaboration of *MEIS2* and AE can be mechanistically linked to kinases, which opens an avenue for targeting this leukemogenic liaison between the two transcription factors by approved drugs such as dasatinib.

Altogether, these data shed light on an unexpected leukemogenic crosstalk between the most frequent fusion gene in AML and the *MEIS2* homeobox gene, identifying *MEIS2* as a potent collaborative leukemogenic partner that affect DNA binding of the most frequent fusion gene in human AML.

EXPERIMENTAL PROCEDURES

Patient Samples, Cell Lines, and Mouse Experiments

Mononuclear cells isolated from diagnostic BM or PB with AML leukemias from 92 adult patients were analyzed ($n = 70$ for t(8;21), $n = 11$ for *PML-RAR α* , $n = 11$ for *inv* (16), and $n = 5$ for *NPM-WT* and *NPMC*). CD34⁺ from bone marrow mononuclear cells (BM MNCs; Lonza) ($n = 13$) from healthy individuals were taken as controls. Cytochemistry and cytogenetics (Table S1) were performed in all cases as described. Cases were classified according to the French-American-British criteria and World Health Organization classification (Bennett et al., 1976; Harris et al., 1999). The study was approved by the ethics committees of all participating institutions, and informed consent was obtained from all patients before they entered the study in accordance with the Declaration of Helsinki (<http://www.wma.net/en/30publications/10policies/b3/index.html>). The t(8;21)-positive AML cell lines Kasumi-1 (all DMSZ) and SKNO-1 (kindly provided by Michael Lübbert, Freiburg, Germany) were used for expression analysis. Kasumi-1 and OCI-AML3 were cultured in RPMI 1640 with 20% fetal bovine serum (FBS) and

1% penicillin-streptomycin. SKNO-1 was cultured in RPMI 1640 medium with 10% FBS + granulocyte-macrophage colony-stimulating factor (GM-CSF) (10 ng/ml). Mice experiments were performed in compliance with the German Law for Welfare of Laboratory Animals and were approved by the Regierungspräsidentium Tübingen, Germany.

Co-immunoprecipitation and Western Blotting

Cell lines HEK293 (ATCC, CRL 1573) and HeLa (ATCC, CCL 2) were grown in DMEM (Gibco) supplemented with 10% fetal calf serum (FCS), penicillin, and streptomycin. HEK293 and HeLa cells were transfected using the Nanofectin transfection reagent (PAA) according to the manufacturer's instructions. For western blotting and immunoprecipitation (IP) experiments whole-cell lysates were prepared as described previously (Salat et al., 2008; Wacker et al., 2011). Protein concentrations were determined using the Bradford assay method (Bio-Rad). Details regarding coIP and western blot can be found in Supplemental Experimental Procedures.

ChIP-Seq and Peak Detection

Chromatin was harvested as described previously (Denissov et al., 2007). ChIP was performed using specific antibodies to AE (Diagenode, C15310197) and analyzed by qPCR or ChIP-seq as previously described (Martens et al., 2012). Primers for qPCR used were as follows:

SP11: forward, 5'-GGGTAAAGAGCCTGTGTACAGC-3'; reverse, 5'-CAGATG CACGTCCTCGATAC-3'
FUT7: forward, 5'-TGAAACCAACCCTCAAGGTC-3'; reverse, 5'-TCACTG GCATGAATGAGAGC-3'
NFE2: forward, 5'-GGTTAGCAGCATACGTGGAG-3'; reverse, 5'-ACGATA CGGAGAAAACACG-3'
OGG1: forward, 5'-CCACCCTGATTCTCATTGG-3'; reverse, 5'-CAACCA CCGCTCATTTACAC-3'
VAV1: forward, 5'-AGAAGGGTTTGAGGGCTAGG-3'; reverse, 5'-CTGTTA CCAGGGCTTGGTTG-3'
H2B: forward, 5'-TGCATAAGCGATTCTATATAAAAGCG-3'; reverse, 5'-AT AAAGCGCAACGAAAGG-3'
MYOG: forward, 5'-AAGTTTGACAAGTTCAAGCACCTG-3'; reverse, 5'-TG GCACCATGCTTCTTAAGTC-3'.

Relative occupancy was calculated as fold over background, for which the second exon of the myoglobin gene or the promoter of the *H2B* gene was used.

Illumina sequencing was done as previously described (Martens et al., 2010). Briefly, end repair was performed using the precipitated DNA of ~30 million cells using Klenow and T4 PNK. A 3' protruding A base was generated using Taq polymerase, and adapters were ligated. The DNA was loaded on gel and a band corresponding to ~300 bp (ChIP fragment + adapters) was excised. The DNA was isolated, amplified by PCR, and used for cluster generation on the Illumina genome analyzer. Fastq files were quality controlled and adaptor trimmed using trimm-galore (Martin, 2011), and sequences with phred score of 20 or higher were considered for downstream analysis. Sequences were then aligned to the human genome version hg19 using bowtie2 (Barbie et al., 2009). Peak calling and annotation was done using CisGenome (Ji et al., 2008) and HOMER v3.12 (<http://homer.salk.edu/homer/ngs/peaks.html>).

RNA-Seq and Analysis

RNA-seq was performed using libraries prepared by TruSeq RNA Sample preparation Kit version 2. The samples were run on HiSeq2000. After trimming Illumina sequencing adapters using trimm-galore (Martin, 2011), high-quality raw Fastq files (phred score of 20 or higher) were aligned using tophat and respective RefSeq files (the human Hg19 assembly and the murine mm10 genome version). Differential expression analysis was performed using Cufflinks (Trapnell et al., 2009, 2010) and R packages (Team, 2013).

ACCESSION NUMBERS

The accession numbers for the microarray, ChIP-seq, and RNA-seq (Kasumi cell and murine leukemic BM samples) are GEO: GSE81174, GSE81321, GSE81328, and GSE81329, respectively.

SUPPLEMENTAL INFORMATION

Supplemental Information includes Supplemental Experimental Procedures, five figures, and eight tables and can be found with this article online at <http://dx.doi.org/10.1016/j.celrep.2016.05.094>.

AUTHOR CONTRIBUTIONS

N.M.V., J.K., F.O., V.N.T., A.M., J.H.A.M., V.P.S.R., L.Q.-M., K.F., S.B., and T.M. performed research and analyzed the data. J.H.A.M. and M.A.W. performed the sequencing analysis. K.S., W.H., K.D., H.D., and H.G.S. contributed research material. N.M.V., J.K., M.A.W., V.P.S.R., M.F.-B., and C.B. contributed to data interpretation. N.M.V. and C.B. wrote the manuscript, and C.B. designed the project.

ACKNOWLEDGMENTS

The authors would like to thank all members of the Core Facility FACS, Core Facility Genomics of the University Ulm and the animal facility of the Helmholtz Centre Munich and the University Ulm for breeding and maintenance of the animals. We want to thank R.K. Humphries for editing the manuscript. The work was supported by grants from the Bundesministerium für Bildung und Forschung (NGFN2 grant 01GS0448), the DFG (SFB 1074 project Z1, project A3 to FO and A6 to M.F.-B. and V.P.S.R.), and the Helmholtz Alliance Preclinical Comprehensive Cancer Center (to C.B.).

Received: December 4, 2014

Revised: April 20, 2016

Accepted: May 27, 2016

Published: June 23, 2016

REFERENCES

- Alharbi, R.A., Pettengell, R., Pandha, H.S., and Morgan, R. (2013). The role of HOX genes in normal hematopoiesis and acute leukemia. *Leukemia* 27, 1000–1008.
- Andreoff, M., Ruvolo, V., Gadgil, S., Zeng, C., Coombes, K., Chen, W., Kornblau, S., Barón, A.E., and Drabkin, H.A. (2008). HOX expression patterns identify a common signature for favorable AML. *Leukemia* 22, 2041–2047.
- Argiropoulos, B., Yung, E., and Humphries, R.K. (2007). Unraveling the crucial roles of Meis1 in leukemogenesis and normal hematopoiesis. *Genes Dev.* 21, 2845–2849.
- Barbie, D.A., Tamayo, P., Boehm, J.S., Kim, S.Y., Moody, S.E., Dunn, I.F., Schinzel, A.C., Sandy, P., Meylan, E., Scholl, C., et al. (2009). Systematic RNA interference reveals that oncogenic KRAS-driven cancers require TBK1. *Nature* 462, 108–112.
- Bennett, J.M., Catovsky, D., Daniel, M.T., Flandrin, G., Galton, D.A., Gralnick, H.R., and Sultan, C. (1976). Proposals for the classification of the acute leukaemias. French-American-British (FAB) co-operative group. *Br. J. Haematol.* 33, 451–458.
- Boissel, N., Renneville, A., Leguay, T., Lefebvre, P.C., Recher, C., Lecerf, T., Delabesse, E., Berthon, C., Blanchet, O., Prebet, T., et al. (2015). Dasatinib in high-risk core binding factor acute myeloid leukemia in first complete remission: a French Acute Myeloid Leukemia Intergroup trial. *Haematologica* 100, 780–785.
- Bürglin, T.R. (1997). Analysis of TALE superclass homeobox genes (MEIS, PBC, KNOX, Iroquois, TGIF) reveals a novel domain conserved between plants and animals. *Nucleic Acids Res.* 25, 4173–4180.
- de Guzman, C.G., Warren, A.J., Zhang, Z., Gartland, L., Erickson, P., Drabkin, H., Hiebert, S.W., and Klug, C.A. (2002). Hematopoietic stem cell expansion and distinct myeloid developmental abnormalities in a murine model of the AML1-ETO translocation. *Mol. Cell. Biol.* 22, 5506–5517.
- Denissov, S., van Driel, M., Voit, R., Hekkelman, M., Hulsen, T., Hernandez, N., Grummt, I., Wehrens, R., and Stunnenberg, H. (2007). Identification of novel functional TBP-binding sites and general factor repertoires. *EMBO J.* 26, 944–954.

- Faber, K., Bullinger, L., Ragu, C., Garding, A., Mertens, D., Miller, C., Martin, D., Walcher, D., Döhner, K., Döhner, H., et al. (2013). CDX2-driven leukemogenesis involves KLF4 repression and deregulated PPAR γ signaling. *J. Clin. Invest.* 123, 299–314.
- Fenske, T.S., Pengue, G., Mathews, V., Hanson, P.T., Hamm, S.E., Riaz, N., and Graubert, T.A. (2004). Stem cell expression of the AML1/ETO fusion protein induces a myeloproliferative disorder in mice. *Proc. Natl. Acad. Sci. USA* 101, 15184–15189.
- Harris, N.L., Jaffe, E.S., Diebold, J., Flandrin, G., Muller-Hermelink, H.K., Vardiman, J., Lister, T.A., and Bloomfield, C.D. (1999). The World Health Organization classification of neoplastic diseases of the hematopoietic and lymphoid tissues. Report of the Clinical Advisory Committee meeting, Airlie House, Virginia, November, 1997. *Ann. Oncol.* 10, 1419–1432.
- Ji, H., Jiang, H., Ma, W., Johnson, D.S., Myers, R.M., and Wong, W.H. (2008). An integrated software system for analyzing ChIP-chip and ChIP-seq data. *Nat. Biotechnol.* 26, 1293–1300.
- Jung, N., Dai, B., Gentles, A.J., Majeti, R., and Feinberg, A.P. (2015). An LSC epigenetic signature is largely mutation independent and implicates the HOXA cluster in AML pathogenesis. *Nat. Commun.* 6, 8489.
- Kawagoe, H., Humphries, R.K., Blair, A., Sutherland, H.J., and Hogge, D.E. (1999). Expression of HOX genes, HOX cofactors, and MLL in phenotypically and functionally defined subpopulations of leukemic and normal human hematopoietic cells. *Leukemia* 13, 687–698.
- Krejci, O., Wunderlich, M., Geiger, H., Chou, F.S., Schleimer, D., Jansen, M., Andreassen, P.R., and Mulloy, J.C. (2008). p53 signaling in response to increased DNA damage sensitizes AML1-ETO cells to stress-induced death. *Blood* 111, 2190–2199.
- Kroon, E., Kros, J., Thorsteinsdottir, U., Baban, S., Buchberg, A.M., and Sauvageau, G. (1998). Hoxa9 transforms primary bone marrow cells through specific collaboration with Meis1a but not Pbx1b. *EMBO J.* 17, 3714–3725.
- Lengerke, C., and Daley, G.Q. (2012). Caudal genes in blood development and leukemia. *Ann. N Y Acad. Sci.* 1266, 47–54.
- Licht, J.D. (2001). AML1 and the AML1-ETO fusion protein in the pathogenesis of t(8;21) AML. *Oncogene* 20, 5660–5679.
- Lo, M.C., Peterson, L.F., Yan, M., Cong, X., Jin, F., Shia, W.J., Matsuura, S., Ahn, E.Y., Komeno, Y., Ly, M., et al. (2012). Combined gene expression and DNA occupancy profiling identifies potential therapeutic targets of t(8;21) AML. *Blood* 120, 1473–1484.
- Maiques-Diaz, A., Chou, F.S., Wunderlich, M., Gómez-López, G., Jacinto, F.V., Rodríguez-Perales, S., Larrayoz, M.J., Calasanz, M.J., Mulloy, J.C., Cigudosa, J.C., and Alvarez, S. (2012). Chromatin modifications induced by the AML1-ETO fusion protein reversibly silence its genomic targets through AML1 and Sp1 binding motifs. *Leukemia* 26, 1329–1337.
- Marcucci, G., Geyer, S., Zhao, J., Carroll, A.J., Bucci, D., Vij, R., Blum, W., Pardee, T., Wetzler, M., Stock, W., et al. (2013). Adding the KIT inhibitor dasatinib (DAS) to standard induction and consolidation therapy for newly diagnosed patients (pts) with core binding factor (CBF) acute myeloid leukemia (AML): initial results of the CALGB 10801 (Alliance) Study. *Blood* 121, 615a.
- Martens, J.H., Brinkman, A.B., Simmer, F., Francoijs, K.J., Nebbioso, A., Ferrara, F., Altucci, L., and Stunnenberg, H.G. (2010). PML-RAR α /RXR Alters the Epigenetic Landscape in Acute Promyelocytic Leukemia. *Cancer Cell* 17, 173–185.
- Martens, J.H., Mandoli, A., Simmer, F., Wierenga, B.J., Saeed, S., Singh, A.A., Altucci, L., Vellenga, E., and Stunnenberg, H.G. (2012). ERG and FLI1 binding sites demarcate targets for aberrant epigenetic regulation by AML1-ETO in acute myeloid leukemia. *Blood* 120, 4038–4048.
- Martin, M. (2011). Cutadapt removes adapter sequences from high-throughput sequencing reads. *EMBnet J.* 17, 200.
- McGonigle, G.J., Lappin, T.R., and Thompson, A. (2008). Grappling with the HOX network in hematopoiesis and leukemia. *Front. Biosci.* 13, 4297–4308.
- Moens, C.B., and Selleri, L. (2006). Hox cofactors in vertebrate development. *Dev. Biol.* 291, 193–206.
- Network, C.G.A.R.; Cancer Genome Atlas Research Network (2013). Genomic and epigenomic landscapes of adult de novo acute myeloid leukemia. *N. Engl. J. Med.* 368, 2059–2074.
- Patel, P.R., Sun, H., Li, S.Q., Shen, M., Khan, J., Thomas, C.J., and Davis, M.I. (2013). Identification of potent Yes1 kinase inhibitors using a library screening approach. *Bioorg. Med. Chem. Lett.* 23, 4398–4403.
- Pineault, N., Buske, C., Feuring-Buske, M., Abramovich, C., Rosten, P., Hogge, D.E., Aplan, P.D., and Humphries, R.K. (2003). Induction of acute myeloid leukemia in mice by the human leukemia-specific fusion gene NUP98-HOXD13 in concert with Meis1. *Blood* 101, 4529–4538.
- Ptasinska, A., Assi, S.A., Mannari, D., James, S.R., Williamson, D., Dunne, J., Hoogenkamp, M., Wu, M., Care, M., McNeill, H., et al. (2012). Depletion of RUNX1/ETO in t(8;21) AML cells leads to genome-wide changes in chromatin structure and transcription factor binding. *Leukemia* 26, 1829–1841.
- Rawat, V.P., Thoenes, S., Naidu, V.M., Arseni, N., Heilmeier, B., Metzeler, K., Petropoulos, K., Deshpande, A., Quintanilla-Martinez, L., Bohlander, S.K., et al. (2008). Overexpression of CDX2 perturbs HOX gene expression in murine progenitors depending on its N-terminal domain and is closely correlated with deregulated HOX gene expression in human acute myeloid leukemia. *Blood* 111, 309–319.
- Rawat, V.P., Humphries, R.K., and Buske, C. (2012). Beyond Hox: the role of ParaHox genes in normal and malignant hematopoiesis. *Blood* 120, 519–527.
- Salat, D., Liefke, R., Wiedenmann, J., Borggrefe, T., and Oswald, F. (2008). ETO, but not leukemogenic fusion protein AML1/ETO, augments RBP-Jkappa/SHARP-mediated repression of notch target genes. *Mol. Cell. Biol.* 28, 3502–3512.
- Schlessl, C., Rawat, V.P., Cusan, M., Deshpande, A., Kohl, T.M., Rosten, P.M., Spiekermann, K., Humphries, R.K., Schnittger, S., Kern, W., et al. (2005). The AML1-ETO fusion gene and the FLT3 length mutation collaborate in inducing acute leukemia in mice. *J. Clin. Invest.* 115, 2159–2168.
- Shen, W.F., Rozenfeld, S., Kwong, A., Köm ves, L.G., Lawrence, H.J., and Largman, C. (1999). HOXA9 forms triple complexes with PBX2 and MEIS1 in myeloid cells. *Mol. Cell. Biol.* 19, 3051–3061.
- Spencer, D.H., Young, M.A., Lamprecht, T.L., Helton, N.M., Fulton, R., O’Laughlin, M., Fronick, C., Magrini, V., Demeter, R.T., Miller, C.A., et al. (2015). Epigenomic analysis of the HOX gene loci reveals mechanisms that may control canonical expression patterns in AML and normal hematopoietic cells. *Leukemia* 29, 1279–1289.
- Team, R.C. (2013). R: A Language and Environment for Statistical Computing (R Foundation for Statistical Computing).
- Thorsteinsdottir, U., Kroon, E., Jerome, L., Blasi, F., and Sauvageau, G. (2001). Defining roles for HOX and MEIS1 genes in induction of acute myeloid leukemia. *Mol. Cell. Biol.* 21, 224–234.
- Trapnell, C., Pachter, L., and Salzberg, S.L. (2009). TopHat: discovering splice junctions with RNA-Seq. *Bioinformatics* 25, 1105–1111.
- Trapnell, C., Williams, B.A., Pertea, G., Mortazavi, A., Kwan, G., van Baren, M.J., Salzberg, S.L., Wold, B.J., and Pachter, L. (2010). Transcript assembly and quantification by RNA-Seq reveals unannotated transcripts and isoform switching during cell differentiation. *Nat. Biotechnol.* 28, 511–515.
- Wacker, S.A., Alvarado, C., von Wichert, G., Knippschild, U., Wiedenmann, J., Clauss, K., Nienhaus, G.U., Hameister, H., Baumann, B., Borggrefe, T., et al. (2011). RITA, a novel modulator of Notch signalling, acts via nuclear export of RBP-J. *EMBO J.* 30, 43–56.
- Westendorf, J.J., Yamamoto, C.M., Lenny, N., Downing, J.R., Selsted, M.E., and Hiebert, S.W. (1998). The t(8;21) fusion product, AML-1-ETO, associates with C/EBP- α , inhibits C/EBP- α -dependent transcription, and blocks granulocytic differentiation. *Mol. Cell. Biol.* 18, 322–333.
- Yan, M., Kanbe, E., Peterson, L.F., Boyapati, A., Miao, Y., Wang, Y., Chen, I.M., Chen, Z., Rowley, J.D., Willman, C.L., and Zhang, D.E. (2006). A previously unidentified alternatively spliced isoform of t(8;21) transcript promotes leukemogenesis. *Nat. Med.* 12, 945–949.

Supplemental Information

MEIS2 Is an Oncogenic Partner

in AML1-ETO-Positive AML

Naidu M. Vegi, Josef Klappacher, Franz Oswald, Medhanie A. Mulaw, Amit Mandoli, Verena N. Thiel, Shiva Bamezai, Kristin Feder, Joost H.A. Martens, Vijay P.S. Rawat, Tamoghna Mandal, Leticia Quintanilla-Martinez, Karsten Spiekermann, Wolfgang Hiddemann, Konstanze Döhner, Hartmut Döhner, Hendrik G. Stunnenberg, Michaela Feuring-Buske, and Christian Buske

Figure S1

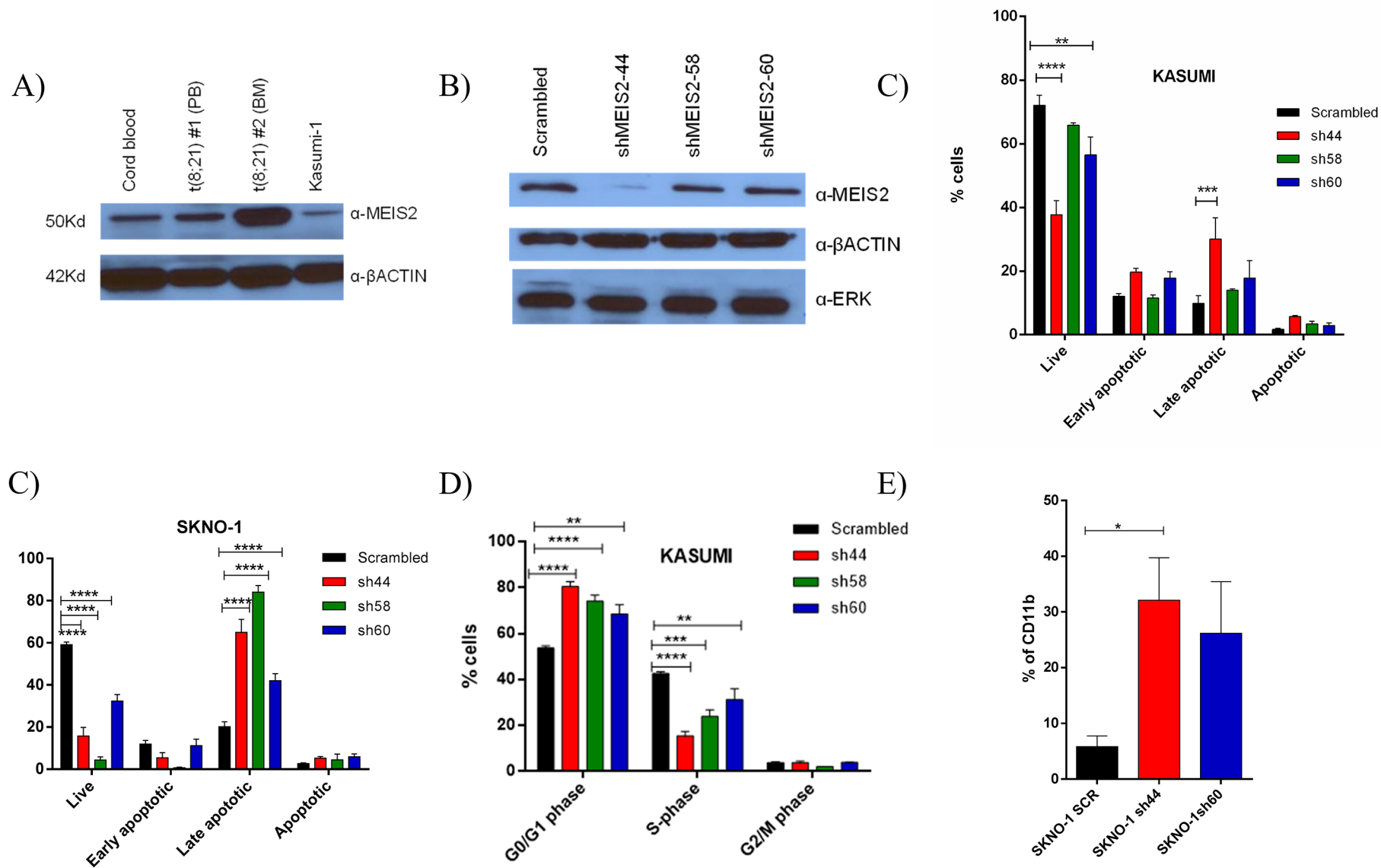


Figure S2

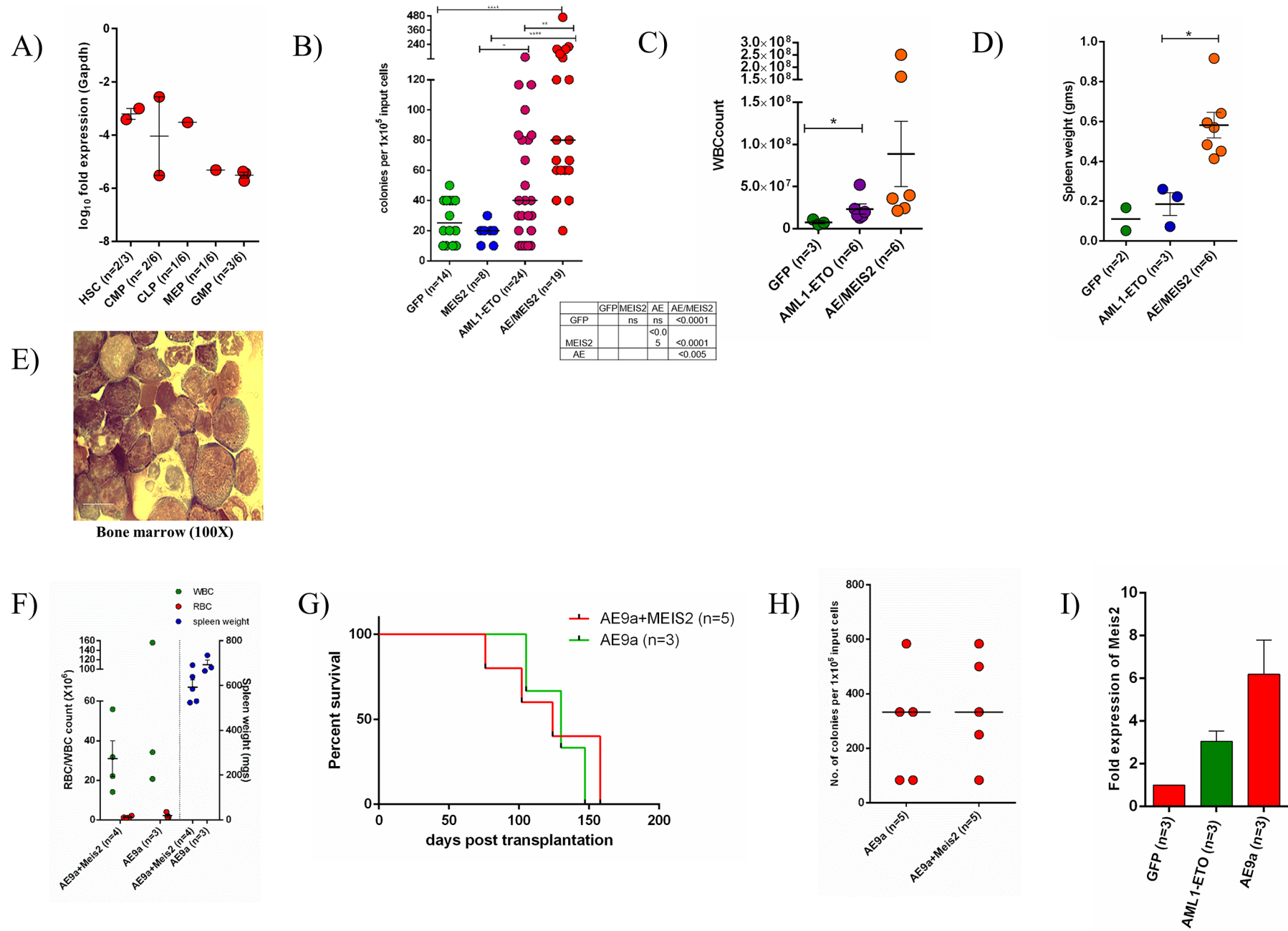
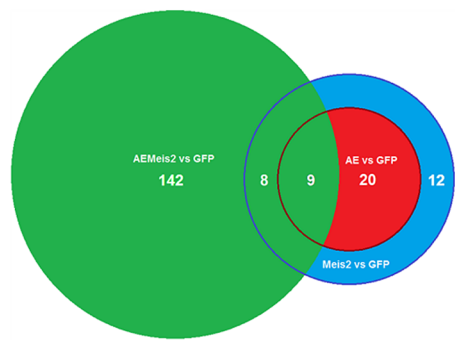
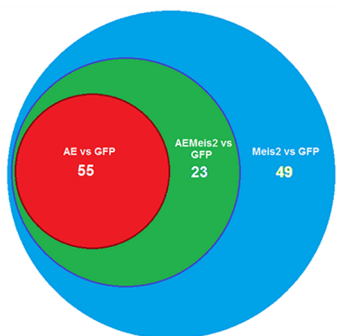


Figure S3

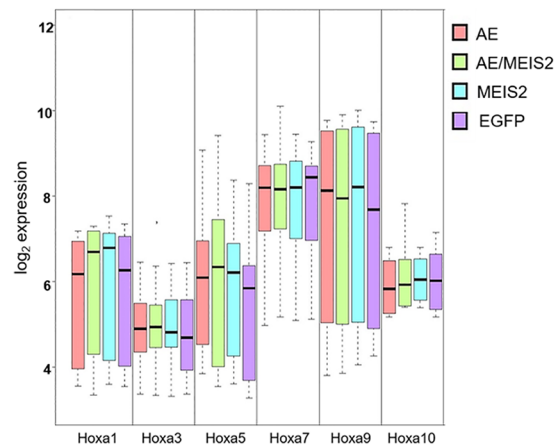
A)



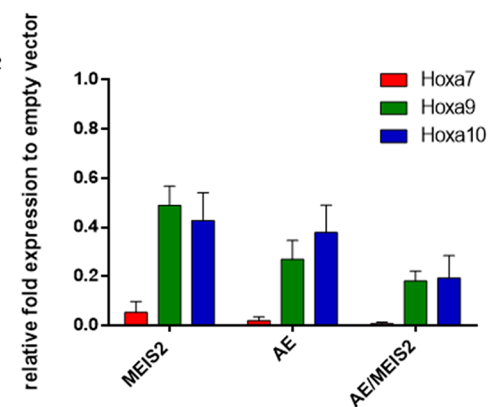
B)



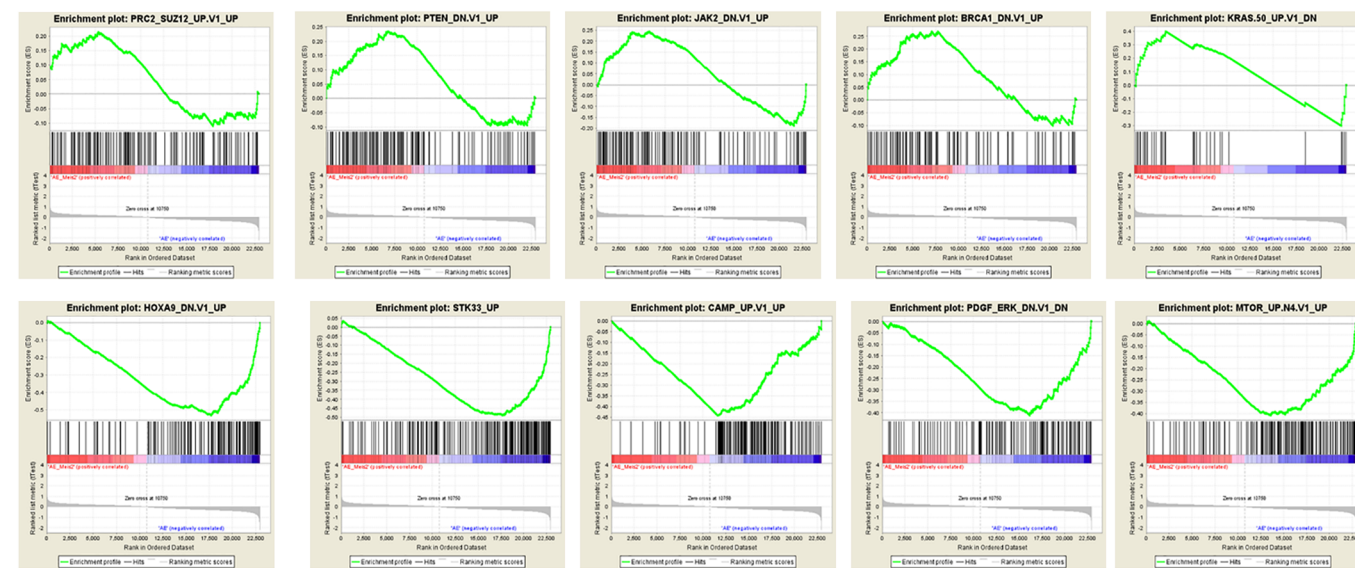
C)



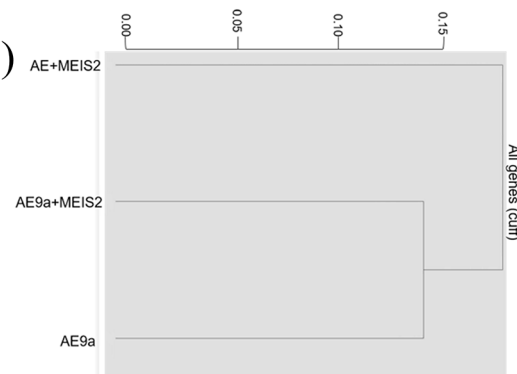
D)



E)



F)



G)

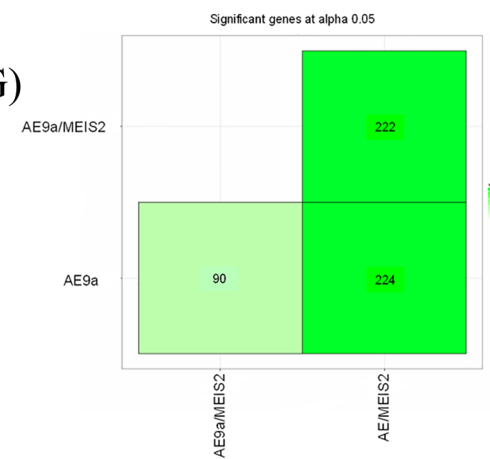


Figure S4

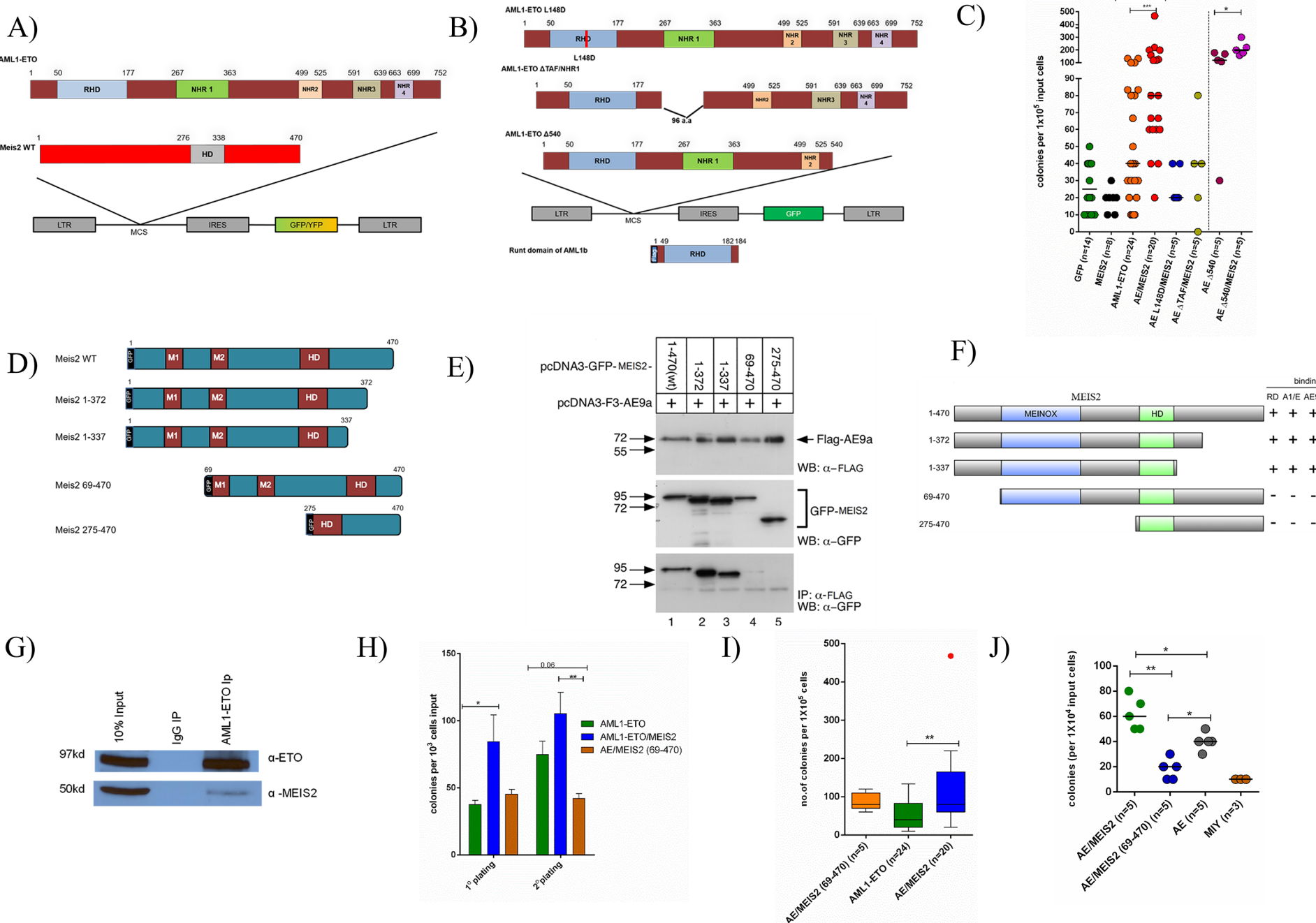
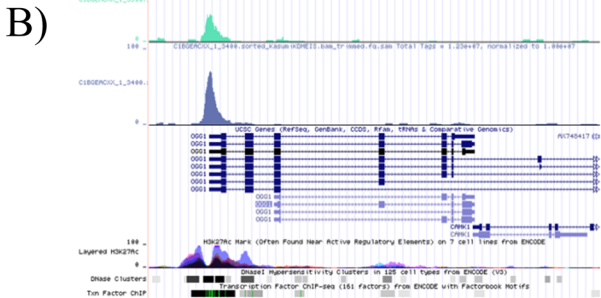
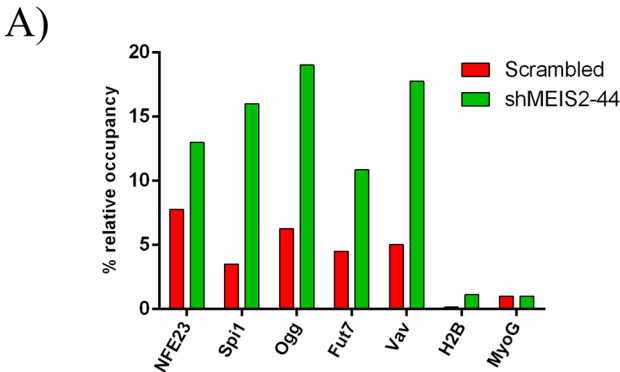
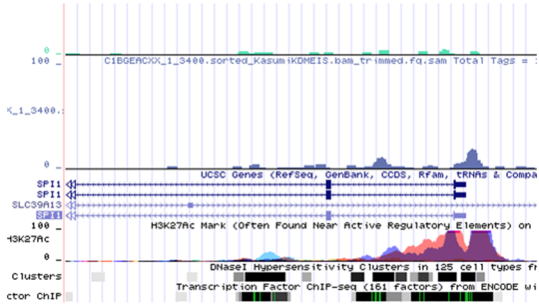


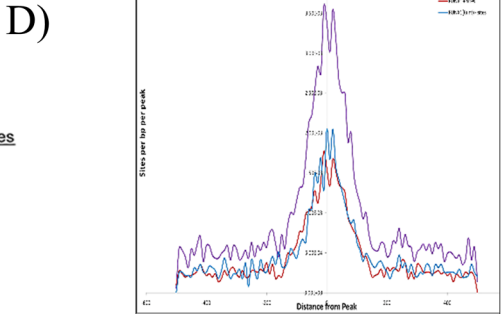
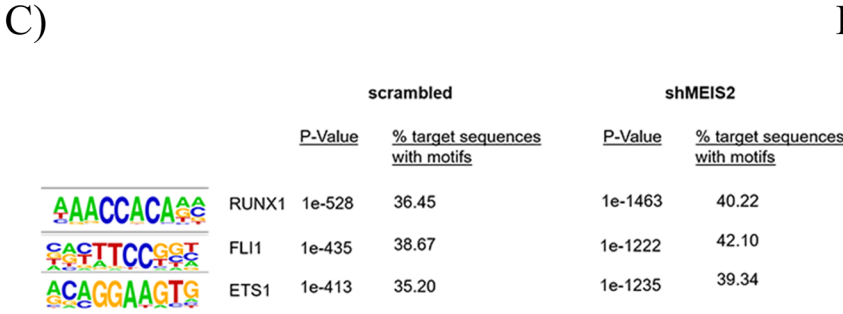
Figure S5



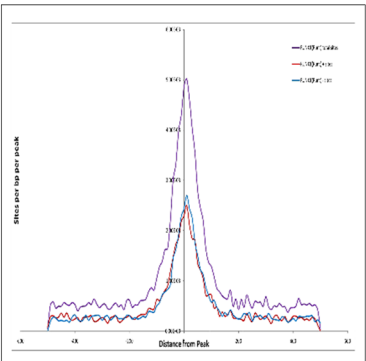
OGG1



SPI1



SCR



shMEIS2

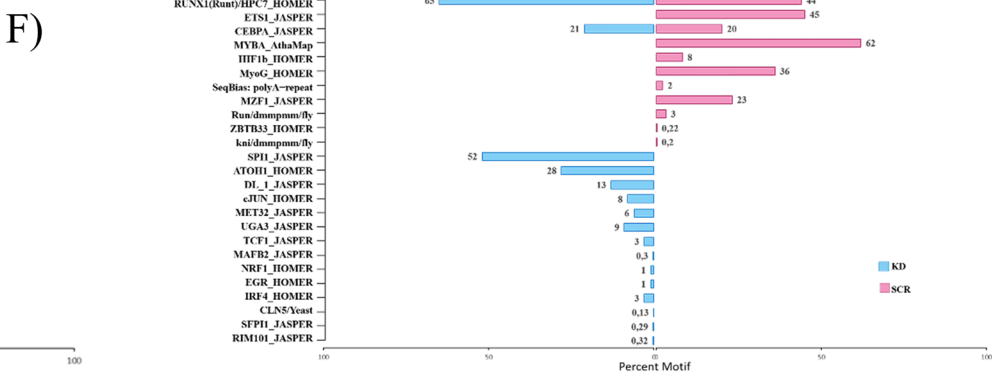
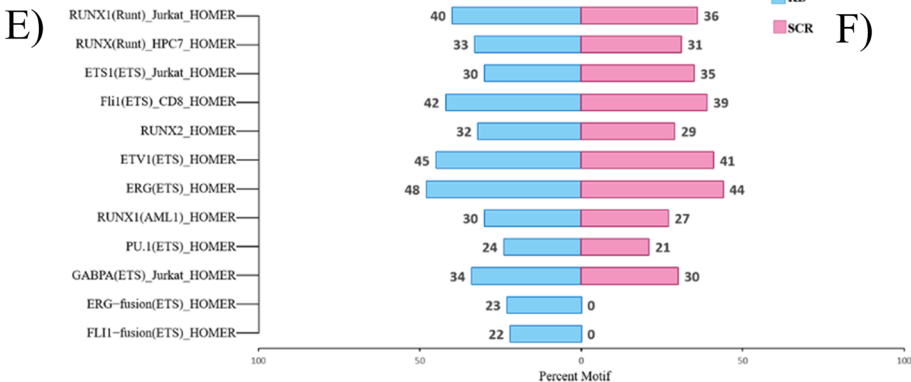
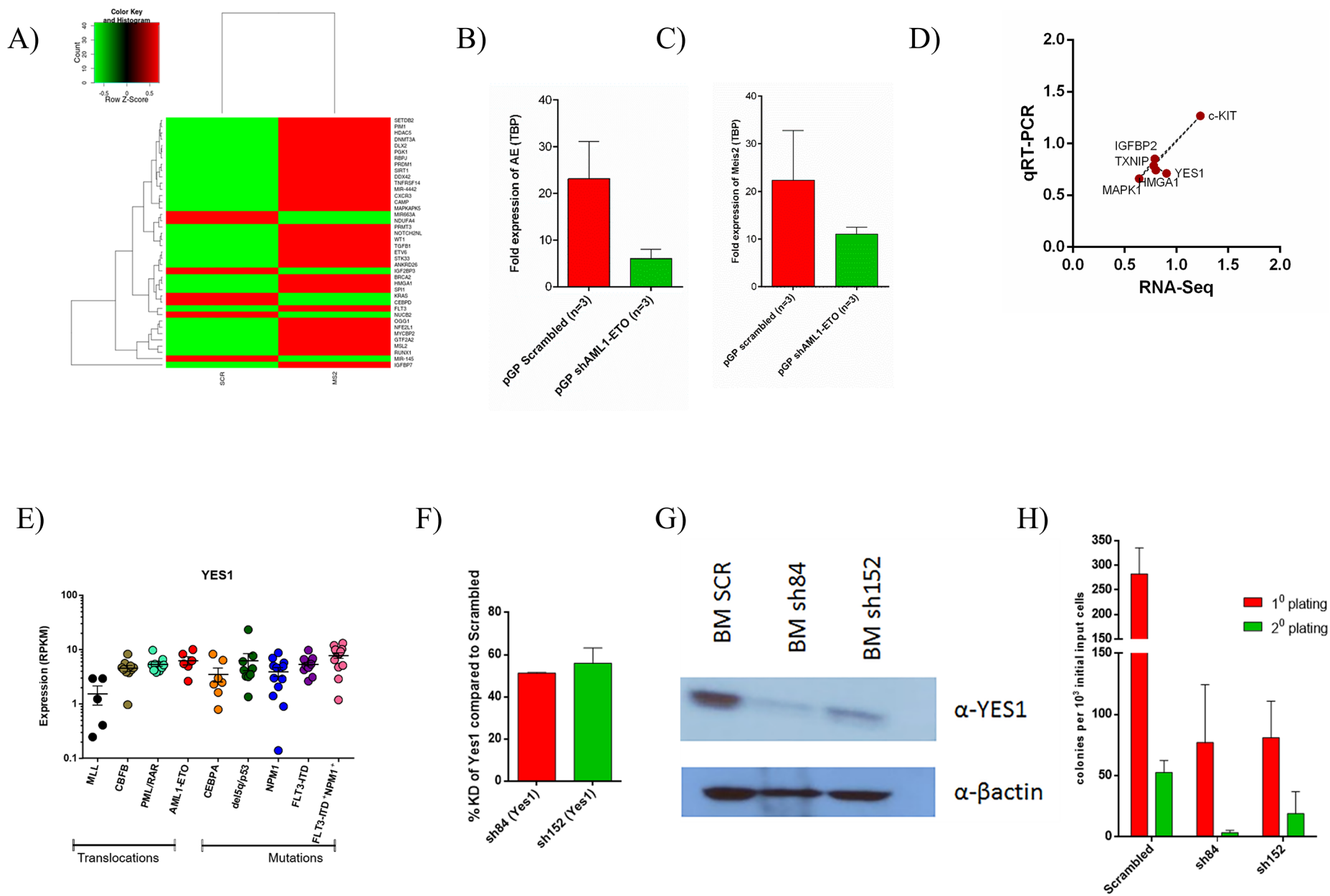


Figure S6



Legends Supplemental Figures:

Figure S1 (related to figure 1 and 2): **A)** Western blot showing the MEIS protein expression in t(8;21) AML samples: MEIS2 protein is highly expressed in both t(8;21) AML samples as well as in bulk cord blood and Kasumi cell line. **B)** Knockdown of MEIS2 protein expression by three different shRNAs compared to scrambled control after puromycin selection). **C)** Apoptosis of Kasumi-1 and SKNO-1 after knockdown of shMEIS2-44 (n=3). **D)** Cell cycle (BRDU) analysis for Kasumi-1 (n=3) and **E)** Differentiation assay for SKNO-1 cells after MEIS2 knockdown showed an increase in CD11b expression (n=3). Bars indicate the mean \pm SEM.

Figure S2 (related to figure 3): **A)** Quantification of *Meis2* expression in murine subpopulations by qRT-PCR. The expression levels of *Meis2* in subpopulations of steady state murine BM (n=3). *Meis2* expression was detected 2 of 3 HSC samples (n= 2/3), 2 of 6 CMP samples (n=2/6), in 1 of 6 CLP and MEP samples (n=1/6) and 3 of 6 GMP (n=3/6) samples. Expression values were normalized to the housekeeping gene *Gapdh* and are shown as mean \pm SEM. HSC=Hematopoietic stem cells; CLP=common lymphoid progenitors; MEP=megakaryocyte-erythroid progenitor; GMP=granulocyte-macrophage progenitor. **B)** Effect of AE and MEIS2 expression on CFU-S number. CFU-S assay was performed by transducing murine BM with the different constructs and were sorted for pure GFP/YFP before transplanting into lethally irradiated mice. The mice numbers indicated are follows (GFP n=14; MEIS2 n=8; AE n=24; AE/MEIS2 n=19). Bar indicated the median of the colonies. Significant differences are marked in the figure and given as a table. CFU-S= colony forming unit-spleen. Haematological parameters of mice transplanted with GFP, AE alone and AE/MEIS2. **C)** White blood cell counts in the PB (significance $^{*}=<0.05$; Mann-Whitney test) and **D)** Spleen weight in transplanted mice (Bars indicate the mean \pm SEM ; significance $^{*}=<0.05$). WBC = white blood cells. **Mice transplanted with BM co-expressing AE9a and MEIS2 developed AML with E)** high blast cell infiltration (magnification of 100X; 20 μ m scale bar) (Giemsa staining) and with **F)** leukocytosis, anemia and splenomegaly (n=5 for AE/MEIS2 and n=3 for AE9a). **G)** Survival of mice. **H)** CFU-S assay was performed with highly purified GFP or GFP/YFP cells expressing AE9a alone (n=5) or AE9a/MEIS2 (n=5). The bar indicates the median colony number, n.s (not significant). **I)** Overexpression of AE and AE9a in 5-FU BM induced a 3 fold and 6fold increase of *Meis2* expression compared to empty vector control (GFP) 96hrs after end of transduction. Bars indicate the mean \pm SEM.

Figure S3 (related to figure 3): **A)** Venn diagram showing the number and overlap of probesets upregulated in the different experimental arms compared to GFP measured by microarray analysis. **B)** Venn diagram showing the number and overlap of probesets downregulated in the different experimental arms compared to GFP measured by microarray analysis. For this analysis, the cutoff was taken as 0.5fold change differential regulation and p value <0.05 . **C)** Box plot for *HoxA* gene expression in BM cells. Expression levels were determined in cells transduced with GFP, AE, MEIS2 and AE/MEIS2 (n=3) by microarrays. Log2 expression was calculated for the *Hox* genes as indicated. **D)** Expression of *Hoxa* genes in 5FU BM transduced cells determined by qRT-PCR. Relative fold expression in comparison to the empty vector was calculated as shown in the figure for BM cells transduced with MEIS2, AE and AE/MEIS2. Bars indicate the mean \pm SEM **E)** GSEA enrichment analysis using the MsigDB ver 5.0 was performed for AE BM and AE/MEIS2 BM for enrichment of oncogenic signature. The upper panel shows the positive correlation of AE/MEIS2 BM towards some top ranked oncogenic signature, lower panel shows the negative correlation of AE BM towards some gene set. **F)** RNA-Seq analysis of leukemic BM: hierarchical dendrogram (right panel) showing the clustering of AE9a and AE9a/MEIS2 samples of leukemic BM from mice transplanted with the different constructs as indicated. **G)** This panel compares the number of significant genes differentially expressed between leukemic BM samples, determined by RNA-Seq and represented as box matrix plot. The number of differentially expressed genes is substantially lower between *AE9a* and AE9a/MEIS2 compared to AE/MEIS2.

Figure S4 (related to figure 3 and 4): **A)** Schematic diagram of constructs. *AE* and *Meis2* were cloned into the multiple cloning sites of the modified MSCV 2.1 vector upstream of the internal ribosomal entry site (IRES) and the enhanced green or yellow fluorescent protein (GFP/YFP) gene. NHR: neryv homology region, HD: Homeodomain, RHD: Runt Homeodomain. **B)** Schematic diagram of AE mutants. The mutants *AE148D*, AE Δ TAF/NHR1, AE Δ 540 were cloned into the multiple cloning sites of the modified MSCV 2.1 vector upstream of the IRES and the GFP/YFP gene. The FLAG-Runt domain was cloned into pCDNA3 expression vector. **C)** Number of CFU-S generated by BM cells expressing *AE* mutants and *Meis2* alone or in combination. The median is given as a bar, Mann - Whitney significance is indicated ($^{***}=<0.001$; $^{**}=<0.005$; $^{*}=<0.05$). **D)** Schematic diagram of *Meis2* (NP_034955) mutants. The GFP-*Meis2* mutants *Meis2* (1-372), *Meis2* (1-337), *Meis2* (69-470) and *Meis2* (275-470) were cloned into pCDNA3 expression vector for Co-IP experiments and the mutant *Meis2* (69-470) was sub-cloned into MSCV retroviral vector for CFU-S assays. **E)** Interaction of MEIS2 with AE9a: co-immunoprecipitation assays were performed on 293 HEK cells to demonstrate interaction of truncated AE protein AE9a with MEIS2. WT MEIS2 and all the mutants interacted strongly with AE9a, RUNT except the N-terminally deleted mutants Δ 1-68 aa (49-470) and 1-274 aa (275-470). **F)** Summary for all interactions: RD: Runt domain, A1/E:AML1-ETO. **G)** IP of AE in the SKNO-

1 cell line and western blot using anti-ETO and anti-MEIS2 antibodies, respectively. IgG normal rabbit antibody is used as IgG control and Thermo Scientific Clean-Blot IP Detection reagent (HRP) was used as secondary antibody to avoid detection-interference from both heavy-chain (approx. 50kDa) and light-chain (25kDa) IgG-fragments of antibodies used for the initial immunoprecipitation assay. **H)** CFC assay with BM cells transduced with the different constructs as indicated. Significance was calculated by the Mann-Whitney test ($*= < 0.05$; $**= < 0.005$) ($n=4$). Bars indicate the mean \pm SEM. **I)** CFU-S assay performed with BM cells transduced with AE/MEIS2 ($n=9$), with AE/MEIS2 (69-470) ($n=5$) and AE alone ($n=7$). Before transplantation transduced cells were highly purified by FACS. The bar indicates the median of colony numbers. Significance was calculated by unpaired t-test with Welch's correction ($**= < 0.005$). **J)** Δ CFU-S assay performed with BM transduced with AE, AE/MEIS2 and AE plus MEIS2 (69-470). Significance was calculated by the Mann-Whitney test ($*= < 0.05$; $**= < 0.005$). The bar indicates the median of the colony numbers.

Figure S5 (related to figure 5): **A)** Bar graph indicating the relative occupancy of known AE targets normalised to the myoglobin control MYOG, which is not bound by AE, after knockdown of MEIS2 compared to SCR; **B)** Peak values of the known AE targets *OGG1* and *SPI1* showing an increase in binding after shMEIS2 compared to SCR (generated from the UCSC genome browser); **C)** Percentage of AE target motifs in Kasumi-1 cells after MEIS2 knockdown and in the SCR control determined by Chip-Seq analysis. **D)** motif distance plot for RUNX1 in Kasumi-1 cells transduced with shMEIS2 versus SCR control. The peaks represent the motif distances for RUNX1. RUNX1+/- are positive and negative strands which sum up for total RUNX1 sites. **E)** Percent known motifs found in Chip-Seq analysis of Kasumi-1 scrambled versus shMEIS2 samples. **F)** Percent imperfect/weaker motifs after de novo motif search (HOMER) in the ChIP-seq data of scrambled versus shMEIS2 Kasumi-1 samples. The motifs were identified using HOMER.

Figure S6 (related to figure 6): **A)** Heat map showing the AE binding occupancies in top ranked genes at the promoter region after MEIS2 knockdown compared to the SCR control. **B)** Knockdown of AE in the SKNO-1 cell line ($> 78\%$) ($n=3$). **C)** Knockdown of AE reduces MEIS2 expression 21 % compared to the scrambled control 6 days post transduction. Fold expression calculated by using ΔC_t values normalized to the housekeeping gene TBP. Bars indicate the mean \pm SEM. **D)** Correlation plot of the expression of genes of interest determined by RNA-Seq versus qRT-PCR in Kasumi-1 cells transduced with the shMEIS2 versus the SCR control. **E)** *YES1* expression levels indicated by RPKM values in AML of different genotypes as determined by RNA-Seq of AML patient samples from TCGA database (Network, 2013). The mean \pm SEM is shown as a bar. RPKM: reads per kilobase of transcript per million reads mapped. **F)** Knockdown of *Yes1* in mouse leukemic BM expressing AE9a/MEIS2. Percent knockdown of *Yes1* (sh84: 51.2% and sh152: 55.9%) compared to scrambled control. **G)** Protein proof of YES1 knockdown in a leukemic BM sample of an AE9a/MEIS2 mouse compared to the scr control. **H)** Colony forming capacity of leukemic BM from AE9a/MEIS2 after *Yes1* knockdown.

Table S1: Patient Characteristics (related to figure 1)

Patient number	Karyotype	Age	Sex	Mutations
AE 1	t(8)(q22),t(21)(q22),+21c	31	M	AE; NRAS
AE 2	t(8)(q22),t(21)(q22),del(9)(q22)	52	F	AE; NRAS
AE 3	t(8)(q22),t(21)(q22),-Y	63	M	AE; CKIT D816
AE 4	t(8)(q22),t(21)(q22),+6,-Y	33	M	AE; FLT3 LM
AE 5	t(8)(q22),t(21)(q22),-Y	41	M	AE; FLT3 LM
AE 6	t(8)(q22),t(21)(q22),-Y	69	M	AE; NRAS; FLT3 D835
AE 7	t(8)(q22),t(21)(q22),-Y	24	M	AE; NRAS
AE 8	t(8)(q22),t(21)(q22),-Y,t(12)8q24,t(17)(q21)	19	M	AE; FLT3 D835
AE 9	t(8)(q22),t(21)(q22)	52	F	AE; CKIT D816
AE 10	t(8)(q22),t(21)(q22),-X	70		AE
AE 11	t(8)(q22),t(21)(q22),-X	45		AE
AE 12	t(8)(q22),t(21)(q22),-Y	25	M	AE; CKIT D816
AE 13	t(8)(q22),t(12)(p11),t(21)(q22),t(17)(q25),del(8)(q23),t(8)(q23)	65	M	AE
AE 14	t(8)(q22),t(21)(q22)	57	F	AE
AE 15	t(8)(q22),t(21)(q22),-X	70	F	AE
AE 16	t(8)(q22),t(21)(q22),+13	78	F	AE
AE 17	t(8)(q22),t(21)(q22),del(9)(q22)	65	M	AE
AE 18	t(8)(q22),t(21)(q22)	38	M	AE
AE 19	t(8)(q22),t(21)(q22), -X	45	F	AE
AE 20	t(8)(q22),t(21)(q22),+8	57	F	AE
AE 21	t(8)(q22),t(21)(q22)	21	M	AE

AE 22	t(8)(q22),t(21)(q22)	51	M	AE
AE 23	t(8)(q22),t(21)(q22),t(20)(p12),t(8)(p12)	64	F	AE
AE 24	t(8)(q22),t(21)(q22)	54	M	AE
AE 25	t(8)(q22),t(21)(q22)	39	M	AE
AE 26	t(8)(q22),t(21)(q22)	31	M	AE
AE 27	t(8)(q22),t(21)(q22),t(1)(p22),t(1)(q23),t(11)(q12),t(3)(q21),t(5)(q33),t(14)(q22)	43	M	AE
AE 28	del(1)(q21),del(1)(q31),t(3)(p21),t(6)(q21),t(3)(q26),t(13)(q21),t(8)(q22),t(21)(q22),del(13)(q21)	73	F	AE
AE 29	t(8)(q22),t(21)(q22)	26	F	AE
AE 30	t(8)(q22),t(21)(q22),-Y,+6	44	M	AE
AE 31	t(8)(q22),t(21)(q22),-Y	61	M	AE
AE 32	t(8)(q22),t(21)(q22),t(1)(p22),t(3)(q21)	41	M	AE
AE 33	t(8)(q22),t(21)(q22)	53	M	AE
AE 34	t(8)(q22),t(21)(q22),+8,del(9)(q22),del(9)(q34)	44	F	AE
AE 35	t(8)(q22),t(21)(q22),t(4)(q12),t(16)(q11),del(9)(q11),-13	28	M	AE
AE 36	t(8)(q22),t(21)(q22),t(7)(q31),t(11),+15	36	M	AE
AE 37	t(8)(q22),t(21)(q22),-X	60	F	AE; FLT3 LM
AE 38	t(8)(q22),t(21)(q22)	41	M	AE
AE 39	t(8)(q22),t(21)(q22),-Y, t(4)(q11),t(20)(p13),t(3)(p24),t(11)(q23),t(2)(q37),t(6)(q23),t(7)(q22),t(9)(q22),t(15)(q24)	62	M	AE
AE 40	t(8)(q22),t(21)(q22),del(9)(q22)	33	M	AE
AE 41	t(8)(q22),t(21)(q22)	52	M	AE; CKIT D816
AE 42	t(8)(q22),t(21)(q22),+8	57	M	AE
AE 43	t(8)(q22),t(21)(q22)	65	F	AE

AE 44	t(8)(q22),t(21)(q22),-Y,t(4)(q11),t(20)(p13),t(3)(p24),t(11)(q23)	62	M	AE
AE 45	t(8)(q22),t(21)(q22),-7	62	F	AE
AE 46	t(8)(q22),t(21)(q22),+8	65	F	AE
AE 47	t(8)(q22),t(21)(q22),del(7)(q31)	77	F	AE; CKIT D816
AE 48	t(8)(q22),t(21)(q22)	45	F	AE; CKIT D816
AE 49	t(8)(q22),t(21)(q22),-Y	78	M	AE
AE 50	t(8)(q22),t(21)(q22),-X	38	F	AE
AE 51	t(8)(q22),t(21)(q22),del(7)(q32)	45	F	AE
AE 52	t(8)(q22),t(21)(q22),-X,-9,-14,-16	32	F	AE
AE 53	t(8)(q22),t(21)(q22),-X	59	F	AE
AE 54	not characterized in detail; not enough metaphases	50	F	AE
AE 55	t(8)(q22),t(21)(q22),-X	29	F	AE
AE 56	t(8)(q22),t(21)(q22)dup(9)(p13;q13),+19	72	M	AE
AE 57	t(8)(q22),t(21)(q22),-Y	20	M	AE
AE 58	t(8)(q22),t(21)(q22),-Y	60	M	AE
AE 59	t(8)(q22),t(21)(q22),-X	24	F	AE
AE 60	t(8)(q22),t(21)(q22),-7,+r	52	F	AE
AE 61	t(8)(q22),t(21)(q22)	66	F	AE,NRAS
AE 62	t(8)(q22),t(21)(q22)	44	M	AE
AE 63	t(8)(q22),t(21)(q22)	33	F	AE
AE 64	t(8)(q22),t(21)(q22),-Y	46	M	AE
AE 65	t(8)(q22),t(21)(q22)	45	F	AE
AE 66	not characterized in detail; not enough metaphases	36	F	AE
AE 67	t(8)(q22),t(21)(q22),-X	69	F	AE
AE 68	t(8)(q22),t(21)(q22),+8,+9	76	M	AE
AE 69	t(8)(q22),t(21)(q22),-X	37	F	AE
AE 70	t(8)(q22),t(21)(q22)	62	F	AE

FLT3-LM = fms-like tyrosine kinase receptor-3 length mutations); NRAS = neuroblastoma RAS viral oncogene homolog; F = female, M = male

Table S2: Characteristics of evaluable transplanted mice (related to figure 3)

	Retroviral construct	Day of sacrifice	RBCs/ml x10⁹	WBCs / ml x 10⁶	SP size (mm)	SP Weight (mg)	% BM Blasts	% SP Blasts	Diagnosis
#1	GFP	90	4.5	11	13x4	52.2	1	0	No disease
#2	GFP	275	5.5	7	14x3	135	0	1	No disease
#3	GFP	119	5.2	5	15x4	167	3	1	No disease
#4	AE	90	1.26	23	27x5	400	n.d	n.d	No disease
#5	AE	178	2	5.2	20x4	270	n.d	0	No disease
#6	AE	126	7	16	23x6	260	6	3	No disease
#7	AE	90	8	13	18x3	223	2	0	No disease
#8	AE9a	147	4	34.2	25x4	735	80	n.d	AML
#9	AE9a	129	1.4	15.4	25x4	680	84	n.d	AML
#10	AE/MEIS2	168	6.38	3.95	23x7	484	18	41	AML
#11	AE/MEIS2	281	5.47	2.45	24x5	570	42	58	AML
#12	AE/MEIS2	274	1.64	3.58	30x9	917	21	57	AML
#13	AE/MEIS2	171	0.84	161	24x4	641	74	n.d	AML
#14	AE/MEIS2	150	1.1	250	23x3	451	71	n.d	AML
#15	AE/MEIS2	119	2.6	21.2	25x4	594	80	67	AML
#16	AE9a/MEIS2	76	nd	nd	25x7	639	60	70	AML
#17	AE9a/MEIS2	124	2.1	22.12	26x4	691	33.7	nd	AML
#18	AE9a/MEIS2	102	1.2	14.16	25x5	585	54	68	AML

Table S3: Immunophenotype of diseased mice (n=3) (related to figure 3)

<i>AML1-ETO/MEIS2*</i>		
	BM	
	Mean	SEM
Gr1⁺	23.23	1.07
Mac1⁺	6.21	3.14
Gr1⁺/Mac1⁺	36.20	17.70
Sca1⁺	4.65	2.75
c-kit1⁺	28.57	7.25
Sca1⁺/c-kit1⁺	5.40	3.09
Ter119⁺	1.31	0.68
B220⁺	4.30	1.89
CD4⁺	17.26	10.69
CD8⁺	0.68	0.29












*the percentage of each cell surface marker is derived from cells that were gated for GFP/YFP positive cells.

Table S4: List of all excel sheets as a tabular form

Microarray data: List of log ₂ fold differentially regulated probesets of BM expressing both <i>AE</i> and <i>Meis2</i> compared to empty vector control <i>GFP</i> A) Probesets belonging to <i>AE/MEIS2</i> vs <i>GFP</i> B) <i>AE</i> vs <i>GFP</i> C) <i>Meis2</i> vs <i>GFP</i> and D) <i>AE</i> vs <i>AE/MEIS2</i>	Sheet 1-4
Gene Set Enrichment Analysis (MsigDB ver 5.0) of microarray data for <i>AE</i> and <i>AE/MEIS2</i> BM: A) GSEA analysis for oncogenic signature for <i>AE</i> BM B) GSEA for oncogenic signature for <i>AE/MEIS2</i> BM	Sheet 5-6
ChIP-Seqencing: A) List of peak scores of Kasumi SCR and B) Kasumi shMEIS2 generated by ChIP-Seqencing (see separate excel file). The peakscores belong to the promoter binding regions of 1kb upstream and 100bp down of the transcriptional start site (TSS).	Sheet 7-8
List of differentially expressed genes after MEIS2 knock-down in Kasumi cells compared to the scrambled control as determined by RNA-Seq (see separate excel file)	Sheet 9
KEGG pathway analysis of differentially expressed genes. Differentially expressed genes in Kasumi cells after shRNA mediated MEIS2 knockdown versus the scr control, obtained from the RNA-Seq data set. The list shows only those pathways with at least 5 differentially expressed genes (see separate excel file).	Sheet 10
List of genes with loss of expression after MEIS2 knockdown in Kasumi cells as determined by RNA-Seq (see separate excel file).	Sheet 11

Table S5: Percent *de novo* motifs as well as weaker motifs derived from Chip-Seq analysis performed for Kasumi-1 scrambled and knockdown MEIS2 cells (related to figure 5).

Kasumi scrambled / Known searched motifs predicated by HOMER

Rank	Motif	P-value	% of Targets	Best Match/Details
1		1e-628	44.32%	RUNX(Runt)
2		1e-475	45.25%	MA0098.1_ETS1
3		1e-92	19.65%	MA0102.2_CEBPA
4		1e-91	62.41%	GAMYB(MYB)
5		1e-70	8.31%	HIF1b(HLH)
6		1e-49	35.66%	MyoG(HLH)
7		1e-30	2.20%	SeqBias: polyA-repeat
8		1e-29	22.68%	MA0056.1_MZF1
9		1e-22	3.01%	Run/dmmpmm(Papat senko)
10		1e-14	0.22%	ZBTB33
11		1e-12	0.20%	kni

Kasumi shMEIS2 de novo searched motifs (weaker motifs)









Rank	Motif	P-value	% of Targets	Best Match/Details
1		1e-1739	65.38%	RUNX(Runt)
2		1e-1498	51.89%	MA0080.2_SPI1
3		1e-203	27.64%	Atoh1(bHLH)
4		1e-191	21.33%	MA0102.2_CEBPA
5		1e-179	12.90%	MA0022.1_dl_1
6		1e-164	7.93%	Jun-AP1(bZIP)
7		1e-96	5.54%	MA0334.1_MET32
8		1e-58	8.57%	MA0410.1_UGA3

Table S6: List of top ranked genes from ChIP-Seq with changes in AE DNA binding occupancies (peak values) after MEIS2 knockdown in Kasumi cells (related to figure 5).

	KSCR*	KshMEIS2
<i>SIRPB2</i>	9.8	15.9
<i>GSK3a</i>	3.7	13.2
<i>CREB1</i>	5.7	17.8
<i>FLT3</i>	3.5	11.3
<i>ASXL1</i>	2.4	16.8
<i>ASXL2</i>	7.3	17.6
<i>HOMER1</i>	8.7	12.5
<i>MAPK6</i>	4.9	11.1
<i>MDM2</i>	7.1	12.8
<i>CDKN2AIPNI</i>	6.1	9.9
<i>HMGAI</i>	9.8	18.5
<i>TAF10</i>	4.9	15.9
<i>Mir-155</i>	4.7	12.7
<i>CBLL</i>	8.7	20

*AE binding to these genes in the scrambled control arm did not meet the defined criteria for binding.

Table S7: KEGG-DAVID pathways*

Category	Term	Count	%	P-Value	Fold Enrichment
KEGG_PATHWAY	hsa03010:Ribosome	62	8.4	7.31E-54	10.81729285
KEGG_PATHWAY	hsa00010:Glycolysis / Gluconeogenesis	11	1.4	0.00515396	2.782835821
KEGG_PATHWAY	hsa04142:Lysosome	16	2.1	0.009072068	2.075774971
KEGG_PATHWAY	hsa04520:Adherens junction	12	1.6	0.01112115	2.365574724
KEGG_PATHWAY	hsa04910:Insulin signaling pathway	17	2.3	0.014794146	1.911442786
KEGG_PATHWAY	hsa00480:Glutathione metabolism	9	1.2	0.01510226	2.732238806
KEGG_PATHWAY	hsa05014:Amyotrophic lateral sclerosis (ALS)	9	1.2	0.021028673	2.577583779
KEGG_PATHWAY	hsa05130:Pathogenic Escherichia coli infection	9	1.21	0.031269501	2.396700707
KEGG_PATHWAY	hsa04810:Regulation of actin cytoskeleton	22	2.9	0.042042053	1.553210691
KEGG_PATHWAY	hsa04612:Antigen processing and presentation	11	1.4	0.043953826	2.011688545
KEGG_PATHWAY	hsa00620:Pyruvate metabolism	7	0.94	0.04436305	2.656343284

*Comparison between MEIS2sh versus Scr Kasumi cells based on RNA-Seq

Table S8: List of selected genes with significant changes in expression and AE binding after MEIS2 knockdown. (related to figure 5)

RNA-Seq (FPKM)					ChIP-Seq (binding occupancies/ peak values)	
Gene id	SCR	shMEIS2	Fold change (log ₂)	p value	SCR	shMS2
<i>CD34</i>	64.3095	80.03	0.315583	0.000296	4.90	5.30
<i>ETV6</i>	20.773	25.16	0.276654	0.002274	17.00	25.00
<i>HMGAI</i>	336.626	268.82	-0.324494	0.000207	9.80	18.50
<i>ICAM1</i>	4.01394	1.52	-1.39637	0.000782	7.30	20.20
<i>IGFBP2</i>	101.188	80.10	-0.337185	0.000802	2.40	6.90
<i>KIT</i>	140.996	173.10	0.29593	3.83E-06	21.80	44.30
<i>MPO</i>	5743.32	7663.06	0.416036	0	17.50	45.10
<i>NUCB2</i>	133.585	187.48	0.489013	1.77E-11	18.40	25.50
<i>PRDM8</i>	48.1844	33.08	-0.542755	3.21E-05	23.60	16.10
<i>TRIB1</i>	10.3546	6.67	-0.635102	0.001671	18.50	38.60
<i>TXNIP</i>	188.487	146.74	-0.361244	3.18E-10	3.40	5.70

Supplemental experimental procedures

Hematopoietic stem and Progenitor cell isolation

Bone marrow (BM) cells were isolated from femora and tibiae of 8-10 week old mice and suspended in Hank's balanced salt solution (HBSS) (Gibco) with 10% fetal bovine serum (FBS) (PAN), 2% Penicillin (5000U/ml)/Streptomycin (5000ug/ml) (PAA). Mononuclear cells were isolated by low density centrifugation (Histopaque 1083, Sigma). Low density mononuclear cells were incubated with CD16/CD32 (clone 2.4G2) antibody followed by a cocktail of biotinylated antibodies containing: anti-CD11b (clone M1/70), anti-B220 (clone RA3-6B2), anti-CD5 (clone 53-7.3) anti-Gr-1 (clone RB6-8C5), anti-Ter119, anti-CD8a (clone 53-6.7) (all from BD Pharmingen); Cells were subsequently incubated with anti-Sca-1 (clone D7) (eBioscience), anti-ckit (clone 2B8) (BD Pharmingen), CD34 (clone RAM34) (ebioscience), FLk-2 (clone A2F10) (ebioscience), CD127 (clone A7R34) (ebioscience), Streptavidin- FITC (BD Pharmingen). Lineage negative cells were isolated by yield sort on a modified 4-laser (405nm, 488nm, 561nm, 633nm) FACS Aria III. Hematopoietic lineages were sorted for purity on a FACS Aria III (BD Biosciences) as follows: HSC (Lineage⁻, ckit⁺, Sca-1⁺, CD34⁺, FLK-2⁺) (Wang et al., 2005), CLP (Lineage⁻, ckit^{low}, Sca-1^{low}, FLK-2⁺, CD127⁺), CMP (Lineage⁻, ckit⁺, Sca-1⁻, CD34⁺, CD16/CD32^{low}) (Karsunky et al., 2008), GMP (Lineage⁻, ckit⁺, Sca-1⁻, CD34⁺, CD16/CD32⁺), MEP (Lineage⁻, ckit⁺, Sca-1⁻, CD34⁺, CD16/CD32⁻) (Akashi et al., 2000).

PCR

Expression of *MEIS2*, *AML1-ETO*, *ETO*, *RUNX1* and *YES1* were assayed by TaqMan® real-time quantitative polymerase chain reaction (real-time qRT-PCR) in total human bone marrow (BM), in AML cell lines and in t(8;21) positive samples as well as from sorted subpopulations from t(8;21) positive AML cases. Human and murine Taqman probes will be provided on request. The relative expression of each gene to the house keeping gene (TBP) was determined by calculating fold change ($2^{-\Delta C_t}$). For linker-mediated PCR (LM-PCR), integrated long-terminal repeats (LTRs) and flanking genomic sequences were amplified and then isolated using a modification of the bubble LM-PCR strategy as previously described (Deshpande et al., 2006; Schessl et al., 2005).

shRNAs, siRNA, cell cycle and apoptosis assay

For stable shRNA mediated knock-down of endogenous MEIS genes, PLKO.1 based lentiviral vectors were used: PLKO.1 empty vector (SHC001), PLKO.1 scrambled (SHC002), PLKO.1-shMEIS2 (TRCN0000016044, TRCN0000024058, TRCN0000024060, GenBank accession no. NM_002399.2), PLKO.1-shYES1 (TRCN0000016111 & TRCN0000010006), PLKO.1-shETO (TRCN0000013666 & TRCN0000013667; NM_004349.2), PLKO.1-shYes1 (TRCN0000339084 & TRCN0000339152; NM_009535.2) (all these validated shRNA's were obtained from Sigma-Aldrich). shRNA mediated knock-down in human cell lines was achieved following the experimental procedure as described previously (Rawat et al., 2010).

siRNA against MEIS2 was performed by using human MEIS2 Accell smart pool siRNA (GE Healthcare Dharmacon, E-011330-00-0005) on human primary AE positive cells. Non-targeting control siRNA was used as control. 5x10⁵ cells were plated in technical triplicates along with siRNAs in a 96 well plate and incubated at 37°C. After 72 hrs the cells were collected and washed; a part of the cells were taken for RNA isolation and measured for MEIS2 KD. 3300 cells were plated in methylcellulose and CFC colonies were counted at day 14 and pooled for determining average absolute cell numbers per colony.

Both cell cycle and apoptosis assays were performed on day 6 of the liquid proliferation assay. Cell cycle analysis was performed after synchronizing the cells (starving with 0.1% RPMI) for 16hrs and 24hrs later flow cytometry was performed by using the APC BrdU flow kit (BD Pharmingen cat#:51-900009AC) and apoptosis assay was performed by using the FITC annexin V apoptosis detection kit (BD Pharmingen: cat#:556547) and were analysed with a FACS Fortessa. For the AE knock down experiments, cells were transduced with shRNA against AE and scrambled control (avg. transduction efficiency 52.6±6.24SEM for SCR and 64.9±9.38SEM for shAE). GFP cells were sorted and analysed 6 days after transduction.

Retroviral and expression plasmids

MSCV based retroviral vectors were used for overexpression AE and Meis2 (Schessl et al., 2005). The *Meis2* construct were purchased from Genecopoeia, Rockville, USA) (Figure S4A). The following AE mutants were used and sub-cloned into the MSCV based retroviral vectors: AE L148D (inactivating the DNA binding domain, by substituting the leucine (L) residue at the DNA binding region of AML1 by aspartic acid (D), AE ATAF (deleting the TAF/NHR1 domain), AE Δ540 (deleting the C-terminal stretch from aa 541 to aa 752) (all constructs kindly provided

by Scott W. Hiebert, Vanderbilt University, Tennessee, USA)(Figure S4B). All *AE* constructs were sub-cloned into the GFP vector, *Meis2* into the YFP vector. *Meis2* was also subcloned into mCherry vector for CFU-S assays. The expression plasmid *pcDNA3-F3-AML1/ETO* was described previously (Denissov et al., 2007; Salat et al., 2008). For co-immunoprecipitation experiments *pcDNA3-GFP-Meis2* was made as follows: *YFP-Meis2* was digested with *EcoRI* and *XhoI*. The insert was purified and ligated into the corresponding sites of *pcDNA3-GFPoStp*, *pcDNA3* (Invitrogen) and *pcDNA3-FLAG1*, respectively, resulting in *pcDNA3-GFP-Meis2*, *pcDNA3-Meis2* and *pcDNA3-FLAG1-Meis2*. The GFP-tag of *pcDNA3-GFP-Meis1* and *pcDNA3-GFP-Meis2* was exchanged by mRuby after digestion with *Acc65I* and *EcoRI* resulting in *pcDNA3-mRuby-Meis1* and *pcDNA3-mRuby-Meis2*. The Runt domain of *AE* (aa 1 to 185) was amplified by PCR using *pcDNA3-F3-AE* as a template and the primers T7L (5'-A T T A T A C G A C T C A C T A T A G G G G A G A C C-3') and Runt_Domain (5'-G C C T C G A G T C A G G A G T G C T T C T C A G T A C G A T T T T C G-3). The PCR product was digested with *EcoRI* and *XhoI* and ligated into the corresponding sites of *pcDNA3-F3*, resulting in *pcDNA3-F3-Runt*. The expression construct *pcDNA3-AE-GFP* was digested with *XhoI* and *EcoRI* to excise the GFP cDNA. pMSCV-Meis2-IRES-YFP was digested with *EcoRI* and *XhoI*. The insert was ligated into the corresponding sites of *pcDNA3-GFPoStp* (Wacker et al., 2011) resulting in *pcDNA3-GFP-Meis2*. This construct was digested with *BamHI/XbaI*, blunted and re-ligated resulting in *pcDNA3-GFP-Meis2* (1-372). The other GFP-Meis2 deletion constructs were made by PCR assisted cloning into the *EcoRI/XbaI* sites of *pcDNA3-GFP-Meis2* using the following primers and GFP-Meis2 as a template: *pcDNA3-GFP-Meis2* (1-337), *Meis2_GFP_UP* (5'-C T C G G C A T G G A C G A G C T G T A C A A G-3'), *Meis2_337_DO* (5'-C G T C T A G A T T A G G G C T G C A C T A T T C T T C T T C T G G C-3'), *pcDNA3-GFP-Meis2* (69-470), *Meis2_69_UP* (5'-C G G A A T T C G T C A A C G A C G C C T T G A A A G A G-3'), *Meis2_DO* (5'-C G T C T A G A C T A T T G G C A T G A A T G T C C A T A A C-3') and *pcDNA3-GFP-Meis2* (275-470), *Meis2_69_UP* (5'-C G G A A T T C G T C A A C G A C G C C T T G A A A G A G-3'), *Meis2_DO*. The Runt domain of AML1/ETO (aa 1 to 185) was amplified by PCR using *pcDNA3-F3-AML1/ETO* as a template and the primers T7L (5'-A T T A A T A C G A C T C A C T A T A G G G A G A C C-3') and Runt_Do (5'-G C C T C G A G T C A G G A G T G C T T C T C A G T A C G A T T T C G-3). The PCR product was digested with *EcoRI* and *XhoI* and ligated into the corresponding sites of *pcDNA3-F3*, resulting in *pcDNA3-F3-Runt*. Co-immunoprecipitation with these constructs was performed as described for the analysis of the AE/MEIS interactions. In another approach, CFU-S assay was performed using the same pGEM-11z-FLAG Meis2 mutant (69-470) construct that was sub-cloned into MSCV-IRES-YFP constructs. The AE9a (MigR1-AE9a) plasmid used for the bone marrow transplantation assay was a gift from Dong-Er Zhang (Addgene plasmid # 12433) (Yan et al., 2006). The lentivirus expression construct for knockdown of AE was cloned into pGreen puro vector (System Biosciences, California, USA) by using siRNA sequences specific for the AE junction region as previously shown (Spirin et al., 2014).

Retroviral transduction and BM transplantation

Stable packaging cell lines were generated for the different constructs and used for BM experiments as reported previously (Deshpande et al., 2006; Schessl et al., 2005). 5-FU BM was transduced with *GFP (control)*, *Meis2*, *AE* alone or with *Meis2*. Successfully transduced BM cells were sorted for GFP, YFP and transplanted into lethally irradiated (0.85 Gy) recipients. Unsorted cells were transplanted in the case of *AE* and *Meis2* co-transduction. As donor mice > 12-week-old (C57Bl/6Ly-Peb3b x C3H/HeJ) F1 (PebC3) mice, as recipients > 8–12 week old (C57Bl/6J x C3H/HeJ) F1 (B6C3) mice were used. The number of transplanted transduced cells ranged from 3×10^5 to 5×10^5 per mouse. In experiments with co-transduced BM cells, a total of 5×10^5 - 1×10^6 and 2×10^6 unsorted cells per mouse were injected for AML1/ETO plus MEIS2, respectively. The median proportion of GFP/YFP double positive cells was and 5 % (1% - 8%) for AE plus MEIS2. Lethally irradiated secondary recipients (0.85 Gy) were injected with 10^6 BM cells from a primary diseased mouse and an equal number of non-transduced BM cells from a syngeneic healthy animal. Colony forming unit assay (CFU) spleen assay was performed by BM transplantation as mentioned above using stable packaging cell lines. GFP/YFP positive BM cells expressing GFP, MEIS2, AE, AE/MEIS2 were transplanted into lethally irradiated mice. For experiments involving the MEIS2 mutant(69-470), 5-FU treated BM cells were transduced after spin infection (2500RPM for 45min) with VCM coated on retronectin ($1 \mu\text{g}/\mu\text{l}$ concentration). Highly purified GFP/YFP/mCherry positive cells were sorted and transplanted into lethally irradiated mice (1.1Gy). For the delta CFU-S assay, GFP/YFP cells were sorted and propagated one week in liquid culture for 7 days. After that day 0 equivalent cell numbers were transplanted into lethally irradiated mice as indicated. Mice were sacrificed after 12 days and analysed for spleen colonies. Additional mouse transplantation experiments were performed co-expressing AE9a and MEIS2 in murine BM cells with transduction efficiencies with

median of 4.3% (range of 10.8% -4.3%) for AE9a and 2.5% to 0.8% for AE9a/MEIS2 and injected 1×10^6 cells per mouse. All the sorting were tested for purity after sorting with more than 95% purity.

Flow cytometry, cell morphology and histopathology analyses

Immunophenotypic analysis of murine single-cell suspensions was performed using a FACS Calibur flow cytometer (Becton Dickinson) and Cell Quest software (Becton Dickinson) as previously described (Deshpande et al., 2006). Antibodies used for fluorescence activated cell sorting (FACS) were labelled with phycoerythrin for Gr-1, CD11b (Mac-1), Sca-1, Ter119, CD4, CD19, and allophycocyanin for CD11b (Mac-1), CD117 (c-kit), B220, and CD8 (BD Pharmingen, Heidelberg, Germany). In t(8;21) positive patients (n=3) and healthy individuals (n=3) highly purified subpopulations stained for CD34⁺/CD38⁻, CD34⁺/CD38⁺ and CD34⁻/CD38⁺ (BD Pharmingen, Heidelberg, Germany) were sorted using FACS Aria III.

Cell morphology was analysed on cytopspins from 5×10^4 - 1×10^5 cells isolated from BM, spleen and PB stained with Wright-Giemsa. For histologic analyses, sections of selected organs were prepared and stained using standard protocols as previously described (Rawat et al., 2008; Schessl et al., 2005). Immunohistochemistry was performed on an automated immunostainer (Ventana Medical Systems) according to the company's protocols for open procedures with slight modifications. The antibody panel used included CD3 (SP7; Thermo Fisher Scientific), CD45R/B220 (BD), MPO (Neomarkers) and Tdt (Dako).

Co-immunoprecipitation (Co-IP) and Western blotting

Co-immunoprecipitation (Co-IP) experiments were carried out as described previously (Martens et al., 2010; Wacker et al., 2011). Briefly, 24 hours after transfection cells were lysed with 700 μ l CHAPS lysis buffer. The extracts were incubated with 40 μ l agarose-conjugated anti-FLAG antibody (M2, Sigma) at 4°C overnight. The precipitates were washed 6 to 8 times with CHAPS lysis buffer and finally resuspended in SDS-polyacrylamide gel loading buffer. For Western blotting the proteins were resolved in SDS-polyacrylamide gels and transferred electrophoretically at room temperature to PVDF membranes (Millipore) for 1 h at 50 mA using a Tris-glycine buffer system. After blotting the membranes were pre-blocked for 1h in a solution of 3% milk powder in PBS-T (0.1% Tween 20 in PBS) before adding antibodies. The following antibodies were used: anti-GFP (7.1/13.1, mouse monoclonal IgG, secondary antibody peroxidase conjugated sheep anti-mouse IgG, NA931V, GE healthcare), anti-FLAG (M5, Sigma; secondary antibody, NA931V, GE healthcare), anti-ETO (goat polyclonal IgG raised against the C-terminus of ETO, sc-9737, Santa Cruz; secondary antibody peroxidase-conjugated rabbit anti-goat IgG, Jackson Immuno Research), anti-PEBP2 β /CBF β (rabbit polyclonal IgG raised against amino acids 1-182 of full length PEBP2 β , sc-20693, Santa Cruz; secondary antibody peroxidase-conjugated donkey anti-rabbit IgG, GE healthcare), anti-MEIS2 (mouse monoclonal IgG, raised against recombinant MEIS2 of human origin, sc-81986, Santa Cruz; secondary antibody, NA931V, GE healthcare). Immunoprecipitation of YES1 was performed according to the manufacturer's protocol (Pierce TM classic magnetic IP; co-IP Kit, Pierce Biotechnology, Rockford, IL, USA), using the mouse monoclonal anti-YES1 antibody (BD biosciences) and secondary antibody goat anti - mouse IgG-HRP (SC-2005); p-YES1 was detected by using rabbit polyclonal anti-p-c-YES1 (tyr537) (SC-130182) and secondary antibody goat anti - rabbit IgG-HRP (SC-2030). Mouse serum (M5905 from Sigma-Aldrich) and goat serum (G9023 from Sigma-Aldrich) were used instead of the anti-YES1 antibody for IP and as IgG control. All proteins were detected by using Amersham ECL western blotting detection reagent (RPN2124), for YES1 Amersham ECL prime western blotting detection reagent (RPN2232) was used (both from GE Health Care Life Sciences). Immunoprecipitation for AML1-ETO in SKNO-1 cells was performed by using anti-ETO (rabbit: Abcam; ab124269) and probed with either anti-ETO (rabbit: Abcam; ab124269) or anti-AML1 (rabbit: Cell signaling; #4334). As secondary antibody goat anti - rabbit IgG-HRP (SC-2054) was used. The membrane was further probed for MEIS2 interaction by anti-MEIS2 (Abcam; ab174270) and clean-IP detection reagent HRP (Thermo scientific#21233). Western blotting for detection of MEIS2 (rabbit; Abcam; ab174270) was performed by using primary antibodies and appropriate secondary antibodies. Similarly, knockdown of MEIS2 in Kasumi-1 and Yes1 in leukemic mouse BM was performed by using anti-MEIS2 (rabbit: Abcam; ab174270) and anti-Yes1 (BD biosciences) with β -ACTIN (Mouse: SC-4778) and p44/42 MAPK (ERK1/2) (rabbit; cell signaling 4695) as housekeeping controls.

Microarray analyses

Transduced BM cells expressing AE/GFP, *Meis2*/YFP and GFP alone (control), and cells co-expressing AE plus *Meis2* were sorted for GFP, YFP or co-expression of GFP/YFP, respectively. 24 hrs after sorting RNA was isolated with the RNeasy micro kit (Qiagen) according to manufactures instructions for microarray analyses. Microarray analyses were performed using AffymetrixGeneChip Mouse Gene 1.0 ST as previously described (Deshpande et al.,

2011). Gene Set Enrichment Analysis (GSEA) of these BM samples for oncogenic signature was performed using published data from MsigDB (ver 5.0) (Subramanian et al., 2005).

Drug Studies

IC₅₀ values for Dasatinib ((BMS-354825; Bristol-Myers, New Jersey, USA) were calculated by treating 2x10⁵ cells in culture with 0.01% DMSO as control, 100nm, 1000nm and 10µm Dasatinb dissolved in DMSO. Cells were counted at 24hrs, 48hrs and 72hrs. IC₅₀ values were calculated using R-statistical package. Log concentrations were plotted against the probit values of ratio of dead cells. A linear regression model was fitted to find the relationship between the concentration and probit values. The IC₅₀ was then estimated from the generated model by extrapolating the 50% probit value to the drug concentration.

Statistical analyses

Data were evaluated using the Student-*t* test for dependent or independent samples. Differences with *P* values less than 0.05 were considered statistically significant. Values mentioned are Mean ± SEM except for murine percent survival and CFU-S (colony forming unit-spleen) colonies where median and range was used. PRISM Graph pad software (La Jolla, California, USA) was used for the analysis and figures and FLOWJO (Tree Star Inc, Ashland, OR, USA) to analyse the FACS plots. A *p*-value of less than 0.05 was considered statistically significant.

References:

- Akashi, K., Traver, D., Miyamoto, T., and Weissman, I. L. (2000). A clonogenic common myeloid progenitor that gives rise to all myeloid lineages. *Nature* *404*, 193-197.
- Denissov, S., van Driel, M., Voit, R., Hekkelman, M., Hulsen, T., Hernandez, N., Grummt, I., Wehrens, R., and Stunnenberg, H. (2007). Identification of novel functional TBP-binding sites and general factor repertoires. *Embo J* *26*, 944-954.
- Deshpande, A. J., Cusan, M., Rawat, V. P., Reuter, H., Krause, A., Pott, C., Quintanilla-Martinez, L., Kakadia, P., Kuchenbauer, F., Ahmed, F., *et al.* (2006). Acute myeloid leukemia is propagated by a leukemic stem cell with lymphoid characteristics in a mouse model of CALM/AF10-positive leukemia. *Cancer Cell* *10*, 363-374.
- Deshpande, A. J., Rouhi, A., Lin, Y., Stadler, C., Greif, P. A., Arseni, N., Opatz, S., Quintanilla-Fend, L., Holzmann, K., Hiddemann, W., *et al.* (2011). The clathrin-binding domain of CALM and the OM-LZ domain of AF10 are sufficient to induce acute myeloid leukemia in mice. *Leukemia* *25*, 1718-1727.
- Karsunky, H., Inlay, M. A., Serwold, T., Bhattacharya, D., and Weissman, I. L. (2008). Flk2+ common lymphoid progenitors possess equivalent differentiation potential for the B and T lineages. *Blood* *111*, 5562-5570.
- Martens, J. H., Brinkman, A. B., Simmer, F., Francoijs, K. J., Nebbioso, A., Ferrara, F., Altucci, L., and Stunnenberg, H. G. (2010). PML-RARalpha/RXR Alters the Epigenetic Landscape in Acute Promyelocytic Leukemia. *Cancer Cell* *17*, 173-185.
- Network, C. G. A. R. (2013). Genomic and epigenomic landscapes of adult de novo acute myeloid leukemia. *N Engl J Med* *368*.
- Rawat, V. P., Arseni, N., Ahmed, F., Mulaw, M. A., Thoene, S., Heilmeier, B., Sadlon, T., D'Andrea, R. J., Hiddemann, W., Bohlander, S. K., *et al.* (2010). The vent-like homeobox gene VENTX promotes human myeloid differentiation and is highly expressed in acute myeloid leukemia. *Proc Natl Acad Sci U S A* *107*, 16946-16951.
- Rawat, V. P., Thoene, S., Naidu, V. M., Arseni, N., Heilmeier, B., Metzeler, K., Petropoulos, K., Deshpande, A., Quintanilla-Martinez, L., Bohlander, S. K., *et al.* (2008). Overexpression of CDX2 perturbs HOX gene expression in murine progenitors depending on its N-terminal domain and is closely correlated with deregulated HOX gene expression in human acute myeloid leukemia. *Blood* *111*, 309-319.
- Salat, D., Liefke, R., Wiedenmann, J., Borggrefe, T., and Oswald, F. (2008). ETO, but not leukemogenic fusion protein AML1/ETO, augments RBP-Jkappa/SHARP-mediated repression of notch target genes. *Mol Cell Biol* *28*, 3502-3512.
- Schessl, C., Rawat, V. P., Cusan, M., Deshpande, A., Kohl, T. M., Rosten, P. M., Spiekermann, K., Humphries, R. K., Schnittger, S., Kern, W., *et al.* (2005). The AML1-ETO fusion gene and the FLT3 length mutation collaborate in inducing acute leukemia in mice. *J Clin Invest* *115*, 2159-2168.
- Spirin, P. V., Lebedev, T. D., Orlova, N. N., Gornostaeva, A. S., Prokofjeva, M. M., Nikitenko, N. A., Dmitriev, S. E., Buzdin, A. A., Borisov, N. M., Aliper, A. M., *et al.* (2014). Silencing AML1-ETO gene expression leads to simultaneous activation of both pro-apoptotic and proliferation signaling. *Leukemia* *28*, 2222-2228.
- Subramanian, A., Tamayo, P., Mootha, V. K., Mukherjee, S., Ebert, B. L., Gillette, M. A., Paulovich, A., Pomeroy, S. L., Golub, T. R., Lander, E. S., and Mesirov, J. P. (2005). Gene set enrichment analysis: a knowledge-based approach for interpreting genome-wide expression profiles. *Proc Natl Acad Sci U S A* *102*, 15545-15550.
- Wacker, S. A., Alvarado, C., von Wichert, G., Knippschild, U., Wiedenmann, J., Clauss, K., Nienhaus, G. U., Hameister, H., Baumann, B., Borggrefe, T., *et al.* (2011). RITA, a novel modulator of Notch signalling, acts via nuclear export of RBP-J. *Embo J* *30*, 43-56.
- Wang, Y. Y., Zhou, G. B., Yin, T., Chen, B., Shi, J. Y., Liang, W. X., Jin, X. L., You, J. H., Yang, G., Shen, Z. X., *et al.* (2005). AML1-ETO and C-KIT mutation/overexpression in t(8;21) leukemia: implication in stepwise leukemogenesis and response to Gleevec. *Proc Natl Acad Sci U S A* *102*, 1104-1109.

Yan, M., Kanbe, E., Peterson, L. F., Boyapati, A., Miao, Y., Wang, Y., Chen, I. M., Chen, Z., Rowley, J. D., Willman, C. L., and Zhang, D. E. (2006). A previously unidentified alternatively spliced isoform of t(8;21) transcript promotes leukemogenesis. *Nat Med* 12, 945-949.